INTERNATIONAL JOURNAL FOR NUMERICAL METHODS IN FLUIDS
Int. J. Numer. Meth. Fluids **31**: 1087–1120 (1999)

FINITE ELEMENT STUDY OF VORTEX-INDUCED CROSS-FLOW AND IN-LINE OSCILLATIONS OF A CIRCULAR CYLINDER AT LOW REYNOLDS NUMBERS

S. MITTAL* AND V. KUMAR

Department of Aerospace Engineering, Indian Institute of Technology, Kanpur, UP 208 016, India

SUMMARY

Vortex-induced vibrations of a circular cylinder placed in a uniform flow at Reynolds number 325 are investigated using a stabilized space–time finite element formulation. The Navier–Stokes equations for incompressible fluid flow are solved for a two-dimensional case along with the equations of motion of the cylinder that is mounted on lightly damped spring supports. The cylinder is allowed to vibrate, both in the in-line and in the cross-flow directions. Results of the computations are presented for various values of the structural frequency of the oscillator, including those that are sub and superharmonics of the vortex-shedding frequency for a stationary cylinder. In most of the cases, the trajectory of the cylinder corresponds to a *Lissajou* figure of 8. *Lock-in* is observed for a range of values of the structural frequency. Over a certain range of structural frequency (F_s), the vortex-shedding frequency of the oscillating cylinder does not match F_s exactly; there is a slight *detuning*. This phenomenon is referred to as *soft-lock-in*. Computations show that this detuning disappears when the mass of the cylinder is significantly larger than the mass of the surrounding fluid it displaces. A self-limiting nature of the oscillator with respect to cross-flow vibration amplitude is observed. It is believed that the detuning of the vortex-shedding frequency from the structural frequency is a mechanism of the oscillator to self-limit its vibration amplitude. The dependence of the unsteady solution on the spatial resolution of the finite element mesh is also investigated. Copyright © 1999 John Wiley & Sons, Ltd.

KEY WORDS: finite elements; unsteady flows; vortex-shedding; flow-induced vibrations; lock-in; soft-lock-in

1. INTRODUCTION

Flow-induced vibration of a circular cylinder has been investigated by various researchers in the past few decades. Most of these efforts are based on laboratory experiments and very few on computational techniques. Some of the phenomena associated with this type of fluid–structure interactions are quite well known and the reference material is available in books, e.g. by Blevins [1] and Chen [2], and in review articles, e.g. by Sarpkaya [3] and King [4]. It is well known that at Reynolds numbers beyond approximately 40, a cylinder placed in a uniform flow experiences alternating lift and drag forces due to vortex-shedding. A cylinder mounted on flexible supports is, therefore, expected to undergo cross-flow and in-line vibrations. Usually, the time-varying component of the lift force is an order of magnitude larger than the time-varying drag force. Therefore, in general, the cylinder oscillations are predominantly in

* Correspondence to: CFD Laboratory, Department of Aerospace Engineering, IIT, Kanpur, UP 208 016, India. E-mail: smittal@iitk.ac.in

CCC 0271–2091/99/231087–34$17.50

Received 6 July 1998
Revised 28 December 1998

the cross-flow direction. For this reason most of the research efforts in the past have been concentrated on cross-flow oscillations. A cylinder that is subjected to forced cross-flow oscillations with an amplitude beyond a certain threshold value exhibits the phenomenon of *lock-in*. The vortex-shedding frequency of the oscillating cylinder changes to the frequency of cylinder vibrations [5]. Similar observations are made for cylinders that are mounted on flexible supports and are allowed to undergo vortex-induced oscillations [6]. The flow field changes significantly as a result of the cylinder oscillations. The same observations were made in a computational study by Mittal and Tezduyar [7]. Flow past cylinders subjected to forced in-line oscillations was studied by Griffin and Ramberg [8]. They observed that two distinct modes of vortex-shedding are present. These observations were confirmed by Chang and Sa [9] using a numerical model. In another computational study, Mittal and Tezduyar [7] observed that a cylinder subjected to in-line oscillations at a certain frequency results in a symmetric mode of vortex-shedding. For a cylinder restricted to cross-flow vortex-induced vibrations, they were able to observe the phenomena of *lock-in* and *hysteresis*. When the Reynolds number lies in a certain range, depending on the initial conditions for the computation, a high or a low oscillation amplitude solution may be realized. *Hysteresis* has been observed by various researchers in the past in laboratory experiments [3] but the exact cause of the phenomenon was not known. While some researchers attributed it to the non-linear springs in the mountings, others suspected it to be a consequence of variable structural damping. Mittal and Tezduyar [7] concluded, through numerical experiments, that *hysteresis* is a consequence of *lock-in*. *Lock-in* occurs only if the vibration amplitude of the cylinder is greater than a certain threshold value [5]. For a certain range of Reynolds number, if the initial condition corresponds to a cylinder vibrating with a large amplitude, i.e. beyond the threshold value for *lock-in*, the vortex-shedding frequency *locks-on* to the structural frequency and one realizes a high-amplitude solution. On the other hand, if one begins with a solution that corresponds to low-amplitude oscillations, i.e. below the threshold required for *lock-in*, a low-amplitude solution is realized. The oscillator parameters, like the mass of the cylinder, damping and stiffness of the spring were chosen to simulate one of the systems of Griffin *et al.* [6] for their experimental investigations. Flow structure in the wake of a cylinder with forced oscillations has been investigated by many other researchers, e.g. Tanida *et al.* [10], Olinger and Sreenivasan [11], Griffin [12], Toebes [13], Lecointe *et al.* [14], Durgin *et al.* [15], Williamson and Roshko [16], Blackburn and Henderson [17], and Ongoren and Rockwell [18,19]. In some of these studies the cylinder is subjected to oscillations at frequencies that are sub- and superharmonics of the natural vortex-shedding frequency for a stationary cylinder.

In this article we report our computational results for flow-induced vibrations of a cylinder that is mounted on flexible supports and is allowed to oscillate in both cross-flow and in-line directions. The computations are restricted to two dimensions. This work is an extension to the investigation by Mittal and Tezduyar [7], who reported results for flow past an oscillating cylinder restricted to cross-flow vibrations. It is well known that the in-line oscillations are significant only if the mass of the cylinder is not too large compared with the mass of the surrounding fluid it displaces. For the same reason, the mass of the oscillator used in the present work is one-hundredth of the one used by Mittal and Tezduyar [7]. The Reynolds number based on the free-stream speed is 325 and computations are carried out for various values of the structural frequency including the sub and superharmonics of the natural vortex-shedding frequency for a stationary cylinder. The computations lead to various interesting observations. As expected, *lock-in* is observed for a range of values of the structural frequency, but in a manner that is slightly different than the

conventional one. Over a certain range of structural frequencies (F_s), when it is slightly larger than the natural vortex-shedding frequency (F_0), the vortex-shedding frequency of the oscillating cylinder does not exactly match the structural frequency; there is a slight *detuning*, which increases as F_s moves away from F_0. We would like to refer to this phenomenon as *soft-lock-in*. This is unlike what one observes in the conventional phenomenon of *lock-in*, where the vortex-shedding frequency of the oscillating cylinder, mounted on flexible supports, exactly matches the natural vortex-shedding frequency. When the mass of the oscillator is increased, our computations show that the vortex-shedding frequency of the oscillating cylinder matches the structural frequency. This suggests that the phenomenon of *soft-lock-in* is associated with oscillators of low non-dimensional mass (non-dimensionalized with the mass of the surrounding fluid displaced by the cylinder). In most of the cases, the trajectory of the cylinder corresponds to a *Lissajou* figure of 8. The frequency of in-line oscillations is twice that of the cross-flow vibrations. Similar observations have been made earlier by researchers during laboratory experiments [1,2]. Another interesting observation that can be made from our computations is regarding the dependence of the unsteady solution on the spatial resolution of the discretization for this class of flow problems. Three different finite element meshes (M1, M2 and M3) of varying spatial resolutions have been employed in the present study. The mesh (M1) with the least number of nodes is fine enough to capture, accurately, the unsteady flow structures for flows with Reynolds numbers in the range of 325. In fact, all the results presented by Mittal and Tezduyar [7] were computed with the same finite element mesh and their results are in excellent agreement with those from laboratory experiments for flows with stationary cylinder. However, in the present work we discovered that for the oscillating cylinder, for certain values of the structural frequency, the resolution provided by mesh M1 is not adequate for accurate computations. Computations with mesh M2 result in qualitatively different time histories than the ones obtained from mesh M1, while they are almost indistinguishable from those obtained with mesh M3. These calculations demonstrate that even though a mesh (e.g. M1 in this case) may be good enough to resolve all the spatial structures at a certain Reynolds number, the same mesh may not provide enough resolution for computing flows involving moving boundaries and interfaces.

The outline of the rest of this paper is as follows. We begin by reviewing the governing equations for incompressible fluid flow and for the motion of a rigid body under the influence of unsteady fluid forces in Section 2. To accommodate the deformation of the spatial domain, we employ the deforming spatial domain/stabilized space–time (DSD/SST) technique introduced by Tezduyar *et al.* [20,21]. The DSD/SST technique is based on the space–time finite element method in which the finite element interpolation functions depend both on space and on time. In this way the deformation of the spatial domain is taken into account automatically. Special mesh-moving schemes, as described by Mittal and Tezduyar [7], are used to accommodate moving boundaries such that remeshing is avoided. To stabilize the computations against spurious numerical oscillations and to enable the use of equal-order interpolation velocity–pressure elements, the Galerkin/least-squares (GLS) stabilization technique is employed. Section 3 describes the finite element formulation incorporating these stabilizing terms. The non-linear equation systems resulting from the finite element discretization of the flow equations are solved using the generalized minimal residual (GMRES) technique [22] in conjunction with diagonal preconditioners. In Section 4 we present our computational results and make some concluding remarks in Section 5.

2. THE GOVERNING EQUATIONS

Let $\Omega_t \subset \mathbb{R}^{n_{sd}}$ and $(0, T)$ be the spatial and temporal domains respectively, where n_{sd} is the number of space dimensions, and let Γ_t denote the boundary of Ω_t. The spatial and temporal co-ordinates are denoted by $\mathbf{x}$ and t. The Navier–Stokes equations governing incompressible fluid flow are

$$\rho\left(\frac{\partial \mathbf{u}}{\partial t} + \mathbf{u}\cdot\nabla\mathbf{u} - \mathbf{f}\right) - \nabla\cdot\boldsymbol{\sigma} = 0 \quad \text{on } \Omega_t \text{ for } (0, T), \tag{1}$$

$$\nabla\cdot\mathbf{u} = 0 \quad \text{on } \Omega_t \text{ for } (0, T). \tag{2}$$

Here ρ, $\mathbf{u}$, $\mathbf{f}$ and $\boldsymbol{\sigma}$ are the density, velocity, body force and the stress tensor respectively. The stress tensor is written as the sum of its isotropic and deviatoric parts

$$\boldsymbol{\sigma} = -p\mathbf{I} + \mathbf{T}, \quad \mathbf{T} = 2\mu\boldsymbol{\varepsilon}(\mathbf{u}), \quad \boldsymbol{\varepsilon}(\mathbf{u}) = \frac{1}{2}((\nabla\mathbf{u}) + (\nabla\mathbf{u})^T), \tag{3}$$

where p and μ are the pressure and viscosity. Both the Dirichlet- and Neumann-type boundary conditions are accounted for, represented as

$$\mathbf{u} = \mathrm{g} \text{ on } (\Gamma_t)_g, \qquad \mathbf{n}\cdot\boldsymbol{\sigma} = \mathbf{h} \text{ on } (\Gamma_t)_h, \tag{4}$$

where $(\Gamma_t)_g$ and $(\Gamma_t)_h$ are complementary subsets of the boundary Γ_t and $\mathbf{n}$ is its unit normal vector. The initial condition on the velocity is specified on Ω_t at $t = 0$

$$\mathbf{u}(\mathbf{x}, 0) = \mathbf{u}_0 \quad \text{on } \Omega_0, \tag{5}$$

where $\mathbf{u}_0$ is divergence free. A solid body immersed in the fluid experiences unsteady forces and in certain cases may exhibit rigid body motion. The motion of the body, in the two directions along the Cartesian axes, is governed by the following equations:

$$\ddot{X} + 2\pi F_s\zeta\dot{X} + (\pi F_s)^2 X = \frac{C_D}{M} \quad \text{for } (0, T), \tag{6}$$

$$\ddot{Y} + 2\pi F_s\zeta\dot{Y} + (\pi F_s)^2 Y = \frac{C_L}{M} \quad \text{for } (0, T), \tag{7}$$

where F_s is the reduced natural frequency of the oscillator, ζ is the structural damping coefficient, M is the non-dimensional mass of the body while C_L and C_D are the instantaneous lift and drag coefficients for the body respectively. The free-stream flow is assumed to be along the x-axis. $\ddot{X}$, $\dot{X}$ and X denote the normalized in-line acceleration, velocity and displacement of the body respectively, while $\ddot{Y}$, $\dot{Y}$ and Y represent the same quantities associated with the cross-flow motion. In the present study, in which the rigid body is a circular cylinder, the displacement and velocity are normalized by the radius of the cylinder and the free-stream speed respectively. The reduced natural frequency of the system, F_s, is defined as $2f_s a/U_\infty$, where f_s is the actual frequency of the oscillator, a is the radius of the cylinder and U_∞ is the free-stream speed of the flow. The non-dimensional mass of the cylinder is defined as $M = m_b/\rho_\infty a^2$, where m_b is the actual mass of the oscillator per unit length and ρ_∞ is the density of the fluid. It may also be expressed as $M = \pi(\rho_s/\rho_\infty)$, where ρ_s is the effective density of the material of the cylinder. The force coefficients are computed by carrying an integration, which involves the pressure and viscous stresses, around the circumference of the cylinder

$$C_{\mathrm{D}} = \frac{1}{\frac{1}{2}\rho_\infty U_\infty^2 2a} \int_{\Gamma_{\mathrm{cyl}}} (\boldsymbol{\sigma}\mathbf{n})\cdot\mathbf{n}_x \, \mathrm{d}\Gamma, \tag{8}$$

$$C_{\mathrm{L}} = \frac{1}{\frac{1}{2}\rho_\infty U_\infty^2 2a} \int_{\Gamma_{\mathrm{cyl}}} (\boldsymbol{\sigma}\mathbf{n})\cdot\mathbf{n}_y \, \mathrm{d}\Gamma. \tag{9}$$

Here $\mathbf{n}_x$ and $\mathbf{n}_y$ are the Cartesian components of the unit vector $\mathbf{n}$, which is normal to the cylinder boundary Γ_{cyl}. These coefficients include the fluid dynamic damping and the added mass effect. The initial conditions for the displacement and velocity of the cylinder are specified at $t = 0$

$$X(0) = X_0, \qquad \dot{X}(0) = \dot{X}_0, \tag{10}$$

$$Y(0) = Y_0, \qquad \dot{Y}(0) = \dot{Y}_0. \tag{11}$$

The equations governing the fluid flow are solved in conjunction with those for the motion of the cylinder. The force acting on the body is calculated by integrating the flow variables on the body surface. The resulting drag and lift coefficients are used to compute the displacement and velocity of the body, which are then used to update the location of the body and the no-slip boundary condition for the velocity field on the body surface.

3. FINITE ELEMENT FORMULATIONS

To accommodate the motion of the cylinder and the deformation of the mesh, the stabilized finite element formulation is employed. In order to construct the finite element function spaces for the space–time method, we partition the time interval $(0, T)$ into subintervals $I_n = (t_n, t_{n+1})$, where t_n and t_{n+1} belong to an ordered series of time levels: $0 = t_0 < t_1 < \cdots < t_N = T$. Let $\Omega_n = \Omega_{t_n}$ and $\Gamma_n = \Gamma_{t_n}$, we then define the space–time slab Q_n as the domain enclosed by the surfaces Ω_n, Ω_{n+1} and P_n, where P_n is the surface described by the boundary Γ_t as t traverses I_n. As is the case with Γ_t, the surface P_n is decomposed into $(P_n)_g$ and $(P_n)_h$ with respect to the type of boundary condition (Dirichlet or Neumann) being imposed. For each space–time slab we define the corresponding finite element function spaces: $(\mathscr{S}^h_{\mathbf{u}})_n$, $(\mathscr{V}^h_{\mathbf{u}})_n$, $(\mathscr{S}^h_p)_n$ and $(\mathscr{V}^h_p)_n$. Over the element domain, this space is formed by using first-order polynomials in space and time. Globally, the interpolation functions are continuous in space but discontinuous in time.

The stabilized space–time formulation for deforming domains is then written as follows: given $(\mathbf{u}^h)_{n-}$, find $\mathbf{u}^h \in (\mathscr{S}^h_{\mathbf{u}})_n$ and $p^h \in (\mathscr{S}^h_p)_n$ such that $\forall \mathbf{w}^h \in (\mathscr{V}^h_{\mathbf{u}})_n$, $q^h \in (\mathscr{V}^h_p)_n$,

$$\begin{aligned}
&\int_{Q_n} \mathbf{w}^h \cdot \rho\left(\frac{\partial \mathbf{u}^h}{\partial t} + \mathbf{u}^h\cdot\nabla\mathbf{u}^h - \mathbf{f}\right) \mathrm{d}\Omega + \int_{Q_n} \boldsymbol{\varepsilon}(\mathbf{w}^h) : \boldsymbol{\sigma}(p^h, \mathbf{u}^h) \, \mathrm{d}Q + \int_{Q_n} q^h \nabla\cdot\mathbf{u}^h \, \mathrm{d}Q \\
&+ \sum_{e=1}^{n_{\mathrm{el}}} \int_{Q_n^e} \frac{1}{\rho}\tau\left[\rho\left(\frac{\partial \mathbf{w}^h}{\partial t} + \mathbf{u}^h\cdot\nabla\mathbf{w}^h\right) - \nabla\cdot\boldsymbol{\sigma}(q^h, \mathbf{w}^h)\right]\cdot\left[\rho\left(\frac{\partial \mathbf{u}^h}{\partial t} + \mathbf{u}^h\cdot\nabla\mathbf{u}^h - \mathbf{f}\right) - \nabla\cdot\boldsymbol{\sigma}(p^h, \mathbf{u}^h)\right] \mathrm{d}Q \\
&+ \sum_{e=1}^{n_{\mathrm{el}}} \int_{Q_n^e} \delta \nabla\cdot\mathbf{w}^h \rho \nabla\cdot\mathbf{u}^h \, \mathrm{d}Q + \int_{\Omega_n} (\mathbf{w}^h)_n^+ \cdot \rho((\mathbf{u}^h)_n^+ - (\mathbf{u}^h)_n^-) \, \mathrm{d}\Omega = \int_{(P_n)_h} \mathbf{w}^h \cdot \mathbf{h}^h \, \mathrm{d}P.
\end{aligned} \tag{12}$$

This process is applied sequentially to all the space–time slabs $Q_1, Q_2, \ldots, Q_{N-1}$. In the variational formulation given by Equation (12), the following notation is being used:

$$(\mathbf{u}^h)_n^{\pm} = \lim_{\varepsilon\to 0} \mathbf{u}(t_n \pm \varepsilon), \tag{13}$$

$$\int_{Q_n} (\cdots)\, \mathrm{d}Q = \int_{I_n} \int_{\Omega_n} (\cdots)\, \mathrm{d}\Omega\, \mathrm{d}t, \tag{14}$$

$$\int_{P_n} (\cdots)\, \mathrm{d}P = \int_{I_n} \int_{\Gamma_n} (\cdots)\, \mathrm{d}\Gamma\, \mathrm{d}t. \tag{15}$$

The computations start with

$$(\mathbf{u}^h)_0^- = \mathbf{u}_0, \tag{16}$$

where $\mathbf{u}_0$ is divergence free.

In the variational formulation given by Equation (12), the first three terms and the right-hand-side constitute the Galerkin formulation of the problem. The series of element-level integrals involving the coefficients τ and δ are the least-squares terms that are added to the basic Galerkin formulation to ensure the stability of the computations. This type of stabilization is referred to as the GLS procedure and is a generalization of the streamline-upwind/Petrov–Galerkin (SUPG) and pressure-stabilizing/Petrov–Galerkin (PSPG) methods [23]. In the current formulation, τ and δ are given as

$$\tau = \left(\left(\frac{2\|\mathbf{u}^h\|}{h} \right)^2 + \left(\frac{4\nu}{h^2} \right)^2 \right)^{-1/2}, \tag{17}$$

$$\delta = \frac{h}{2} \|\mathbf{u}^h\| z, \tag{18}$$

where

$$z = \begin{cases} \left(\dfrac{Re_u}{3} \right) & Re_u \leq 3 \\ 1 & Re_u > 3 \end{cases},$$

and Re_u is the cell Reynolds number. Both stabilization terms are weighted residuals and therefore maintain the consistency of the formulation. The sixth term in Equation (12) enforces weak continuity of the velocity field across the space–time slabs.

The equations of motion for the oscillator given by Equations (6)–(11) are also cast in the space–time formulation in the same manner as described in the work by Tezduyar *et al.* [21] and Mittal [24].

4. NUMERICAL SIMULATIONS

All the computations reported in this article are carried out on the *Digital* workstations at *IIT Kanpur* in 64-bit precision. Equal-in-order basis functions for velocity and pressure, which are bilinear in space and linear in time, are used and a $2 \times 2 \times 2$ Gaussian quadrature is employed for numerical integration. The non-linear equation systems resulting from the finite element discretization of the flow equations are solved using the GMRES technique [22] in conjunction with diagonal preconditioners. The cylinder resides in a rectangular computational domain whose upstream and downstream boundaries are located at 8 and 22.5 cylinder diameters from the center of the cylinder respectively. The upper and lower boundaries are placed at 8 diameters from the center of the cylinder. The no-slip condition is specified for the velocity on

the cylinder wall and free-stream values are assigned for the velocity at the upstream boundary. At the downstream boundary, we specify a Neumann-type boundary condition for the velocity, which corresponds to zero viscous stress vector. On the upper and lower boundaries, the component of velocity normal to and the component of stress vector along these boundaries are prescribed zero value. Reynolds number, based on the diameter of the cylinder, free-stream velocity and the viscosity of the fluid is 325. The non-dimensional mass M of the cylinder is 4.7273 and the structural damping coefficient is 3.3×10^{-4}. While the mass of the oscillator in the present study is one-hundredth the value considered by Mittal and Tezduyar [7], the damping coefficient has the same value. The lower mass of the oscillator is considered here to encourage the in-line oscillations. The parameters for the oscillator used by Mittal and Tezduyar [7] correspond to the values for one of the models employed by Griffin *et al.* [6] for their experimental investigations. The behavior of the oscillator observed from computations of Mittal and Tezduyar [7] and laboratory experiments of Griffin *et al.* [6] are qualitatively similar. The discrepancy in the magnitude of the various observed quantities can be attributed to the three-dimensionality of the flow and the turbulent wake that is expected at such Reynolds numbers. As in the previous work, the present computations are restricted to two dimensions and to low Reynolds number ($= 325$). Flows at larger Reynolds number are also being computed and will be reported in a later article. Computations are carried out for various values of the non-dimensional structural frequency of the system including those that are sub and superharmonics of the natural vortex-shedding frequency for the stationary cylinder. The effect of the mass M of the oscillator is also investigated for some cases. In all the cases, first the steady state solution is computed for flow past a stationary cylinder at Re 325. This solution is then perturbed by applying, on the cylinder surface, a belt-type boundary condition that consists of a set of counter-clockwise and clockwise rotations. Computations are carried out until a periodic solution develops. The unsteady solution for the flow past the stationary cylinder is used as an initial condition for computing the flow past the oscillating cylinder. The computations are carried out using three finite element meshes. Mesh M1 consists of 4209 nodes and 4060 elements, mesh M2 consists of 7332 nodes and 7126 elements, while mesh M3 has 11706 nodes and 11448 elements. A view of the various meshes is shown in Figure 1. The mesh-moving scheme is same as the one used by Mittal and Tezduyar [7].

Figure 2 shows the summary of the computed results. It shows the variation of the non-dimensional cross-flow and in-line oscillation amplitudes, amplitudes of the unsteady components of the lift and drag coefficients, mean drag coefficient and the vortex-shedding frequency with respect to the structural frequency of the oscillator. The data related to the stationary cylinder are also shown in the same figure. It can be observed from the figure that, as has been reported by various researchers in the past, the motion of the cylinder alters the flow field significantly. This effect manifests itself in the aerodynamic forces experienced by the cylinder and the related Strouhal number for the vortex-shedding frequency. When the structural frequency (F_s) of the oscillator is close to the natural shedding frequency of the cylinder, one observes the phenomenon of *lock-in*; the cylinder vibrates with a large amplitude and the vortex-shedding frequency locks on to the structural frequency. The range of structural frequency over which *lock-in* takes place depends on a number of factors, e.g. the structural damping coefficient, the Reynolds number and the mass of the oscillator. In the present case, the phenomenon of *lock-in* occurs but in a manner that is different than what has been observed in earlier studies. It is observed from Figure 2 that when the structural frequency lies in a certain range which is close to the natural vortex-shedding frequency for the stationary cylinder, the cylinder oscillates with a large cross-flow vibration amplitude. However, over a certain range of structural frequency, when F_s is slightly larger than the natural

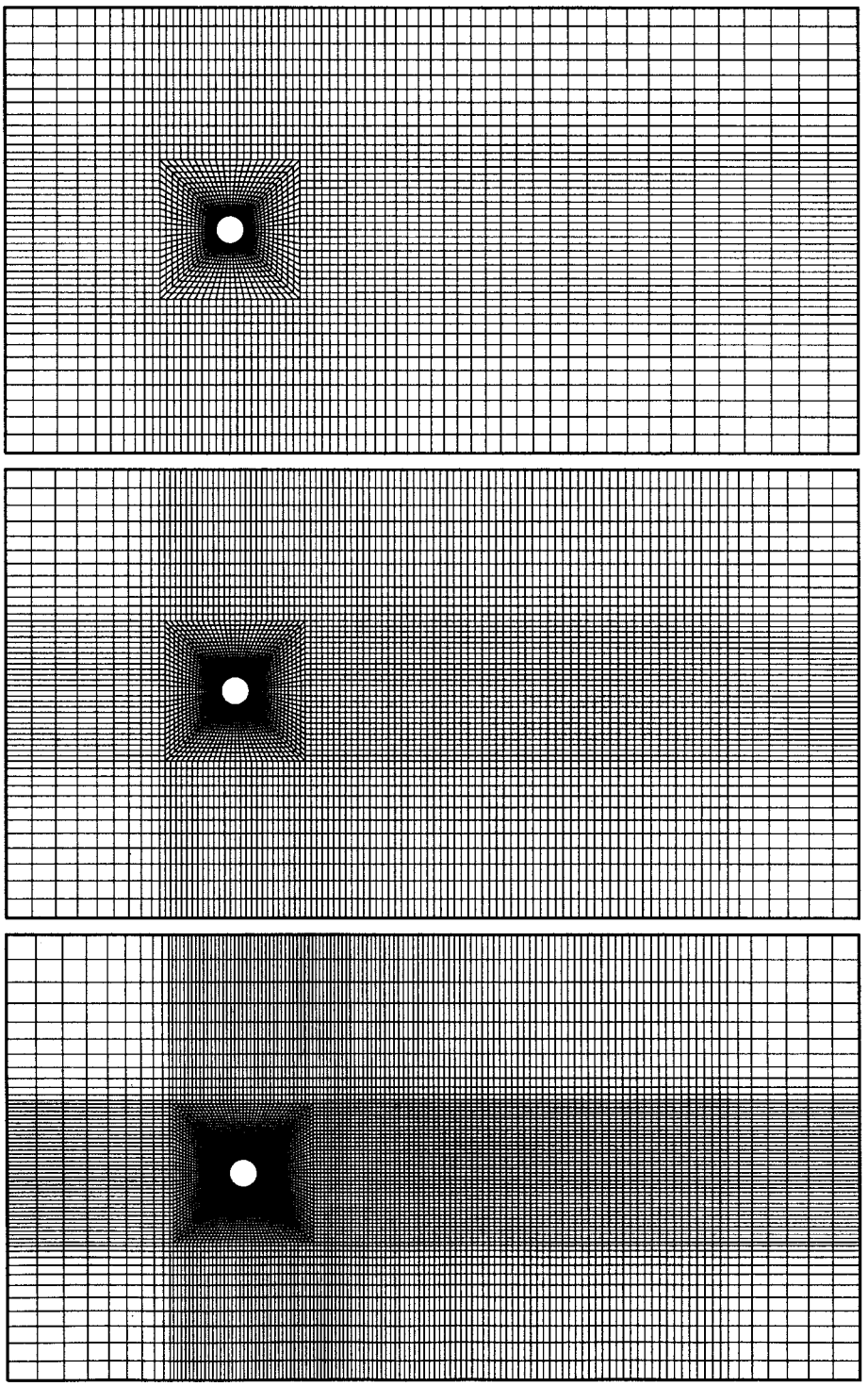

Figure 1. $Re = 325$ flow past a cylinder: finite element meshes; (top) mesh M1 with 4209 node and 4060 elements, (middle) mesh M2 with 7332 nodes and 7126 elements and (bottom) mesh M3 with 11706 nodes and 11448 elements.

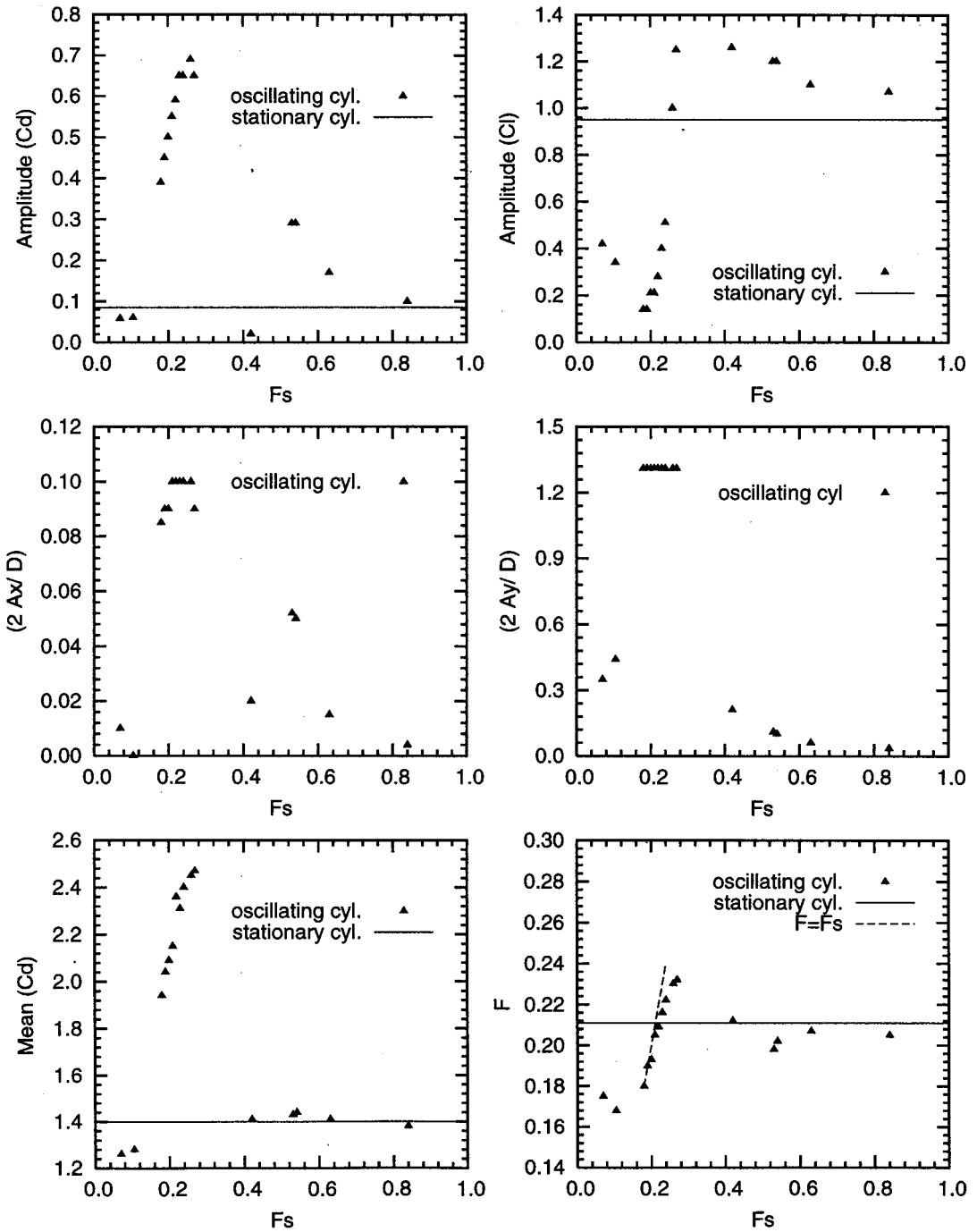

Figure 2. $Re = 325$ flow past an oscillating cylinder: variation of the amplitudes of the unsteady components of the drag and lift coefficients, non-dimensional in-line ($2A_x/D$) and cross-flow ($2A_y/D$) oscillation amplitudes, mean drag coefficient and the vortex-shedding frequency (F) with respect to the structural frequency (F_s) of the oscillator.

vortex-shedding frequency (F_0), the vortex-shedding frequency of the oscillating cylinder does not exactly match the structural frequency; there is a slight *detuning* that increases as F_s moves away from F_0. We would like to refer to this phenomenon as *soft-lock-in*. This is unlike what one observes in the conventional phenomenon of *lock-in* where the vortex-shedding frequency of the oscillating cylinder, mounted on flexible supports, exactly matches the structural frequency. As expected, the cross-flow vibration frequency of the oscillator assumes the same value as the vortex-shedding frequency. In an earlier work, Mittal and Tezduyar [7] had reported computational results for the flow-induced vibration of a circular cylinder using the same finite element formulation as the one used in this article and for a similar range of Reynolds numbers. However, in that work the mass of the cylinder was much larger and the motion of the oscillator was restricted to cross-flow vibrations. A *lock-in* of the conventional type was observed by them. The difference between their results and the present ones can, therefore, be attributed to either the lower mass of the oscillator or the presence of in-line oscillations. Our computations with the cylinder vibrations restricted to the cross-flow direction still result in *soft-lock-in*. When the mass of the oscillator is increased while it is free to vibrate, both in the cross-flow and in the in-line directions, a conventional *lock-in* is observed, which suggests that it is the lower mass of the oscillator that is responsible for *soft-lock-in*. More details on this phenomenon will be given later in the article.

It can also be seen from Figure 2 that the large amplitude vibrations of the cylinder lead to an increased mean and temporally fluctuating drag coefficient. In most of the cases, except for large values of the structural frequency, the vibrations in the cross-flow direction are significantly larger than the ones in the in-line direction. While the variation of amplitude of cross-flow vibrations with structural frequency shows only one peak, the variation of amplitude of in-line oscillations shows two peaks, one close to the natural vortex-shedding frequency and the other at approximately 2.5 times the first one. This is consistent with the behavior of cross-flow and in-line vibrations reported in the review article by King [4]. He reports that the cross-flow oscillations in air occur in the range of $0.125 < F_s < 0.21$, while in water the excitation range increases to $0.1 < F_s < 0.22$. The in-line oscillations, in water, are contained within two adjacent but separate instability regions. The first region is in the range $0.26 < F_s < 0.37$, while the second one is $0.4 < F_s < 0.8$. The first region is associated with the antisymmetric mode of vortex shedding while the second one is characterized by symmetric vortex-shedding, where a pair of counter-rotating vortices is shed from the opposite sides of the cylinder. This symmetric mode of vortex shedding was also observed by Mittal and Tezduyar [7] for forced in-line oscillations of a cylinder with an amplitude of one cylinder radius at $Re = 100$. In the present computations, the second region of instability for the in-line oscillations occurs around $F_s = 0.53$ and is associated with the anti-symmetric mode of vortex-shedding, unlike the observations by King. However, it should be noted that the results reported by King are for high-Reynolds number flows. An interesting experimental study was conducted by Ongeron and Rockwell [18,19] in which they investigated the mode competition in the near wake of an oscillating cylinder for Reynolds numbers in the range $584 < Re < 1300$. They observed that the various vortex-shedding modes can be categorized into two basic groups: symmetrical vortex-formation and anti-symmetrical vortex-formation. There are four basic anti-symmetric modes and only one symmetric mode. The symmetric mode is observed in some of the cases when the cylinder is subjected to forced oscillations at a frequency that

Figure 3. $Re = 325$ flow past an oscillating cylinder: vorticity and pressure fields for the temporally periodic solution at the peak value of the lift coefficient for various values of F_s. The top row is for stationary cylinder. Values of F_s from second row onwards are $F_0/3$, $F_0/2$, F_0, $2F_0$, $3F_0$ and $4F_0$.

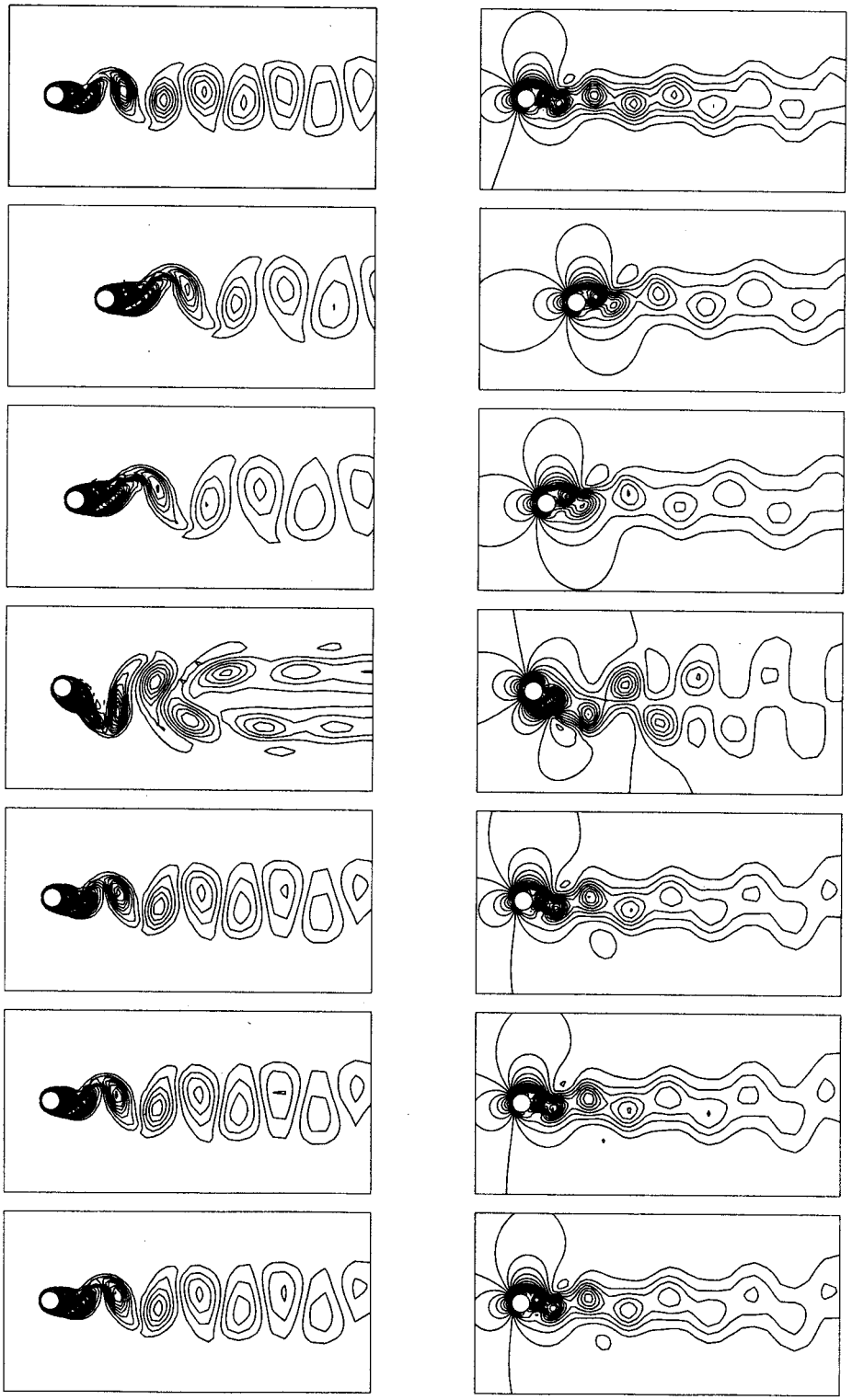

is a superharmonic of the natural vortex-shedding frequency. However, when the angle of oscillations with respect to the free-stream is close to 90°, i.e. the cylinder is subjected to predominantly cross-flow oscillations, it is mostly the anti-symmetric mode of vortex-shedding that is preferred. The results from present computations are consistent with this observation. This suggests that the phenomenon is quite sensitive to the Reynolds number and further investigation is needed to understand it. Blackburn and Henderson [17] have also observed Reynolds number dependence in the vortex-shedding patterns in flow past an oscillating cylinder.

4.1. Re = 325 flow past a stationary cylinder

An unsteady solution for flow past a stationary circular cylinder at $Re = 325$ is computed and is later used as an initial condition for the cases involving oscillating cylinders. Flow past a circular cylinder at $Re = 100$ has become a standard benchmark problem and various researchers in the past have reported their computed results, which are in good agreement with experimental observations [23–26]. Results for flow at $Re = 100$ computed with formulations similar to the one used in this article are in excellent agreement with experimental observations [24]. The finite element mesh M1 is utilized for the computations of the present case. The top row in Figure 3 shows the vorticity and pressure fields for the temporally periodic solution at the peak value of the lift coefficient. Figure 4 shows the time histories of the drag and lift coefficients and their power spectra. The Strouhal number corresponding to the dominant frequency of the lift variation is 0.21 and the mean drag coefficient is 1.4. Our computational results overpredict, slightly, both the quantities compared with the experimental results [27]. It has been observed in the past by various researchers [28–30] that two-dimensional computations tend to overpredict the mean drag coefficient and the Strouhal number, while results from three-dimensional computations are closer to experimental observations. It is also well known that beyond a Reynolds number of approximately 300, the three-dimensional effects in the wake of the cylinder become significant [31]. This suggests that, to get a true picture of the

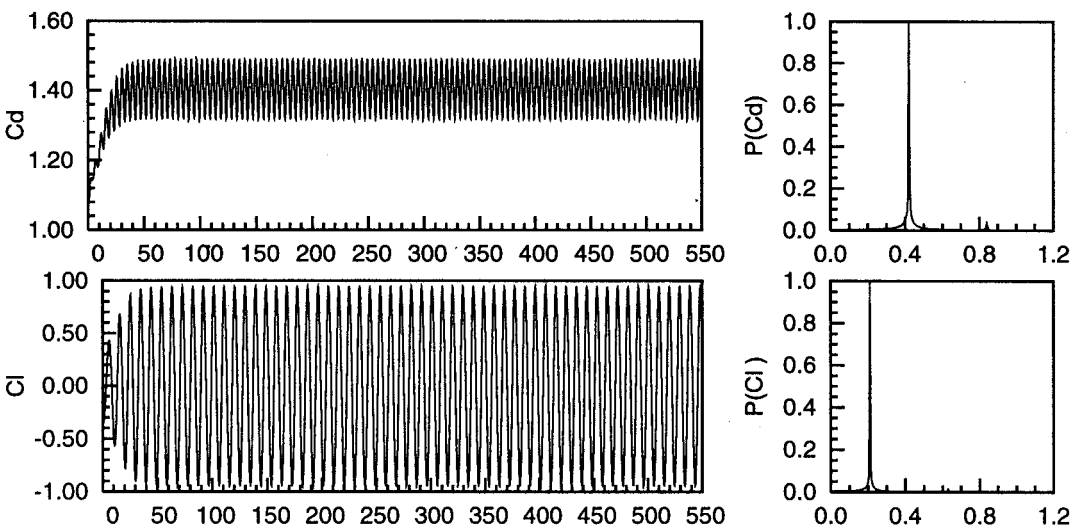

Figure 4. $Re = 325$ flow past a stationary cylinder: time histories of the drag and lift coefficients and their power spectra.

phenomenon, one must carry out three-dimensional computations. However, due to the constraints of the available computational resources, simulations reported in this article are restricted to two-dimensional cases only, with the understanding that these represent the real life situations in an approximate sense. The Strouhal number corresponding to the vortex-shedding for this case will be referred to as the natural vortex-shedding frequency (F_0) in the rest of the article.

4.2. *Re = 325 flow past an oscillating cylinder: effect of structural frequency, F_s*

A fairly comprehensive study of flow-induced vibrations of a circular cylinder was reported by Mittal and Tezduyar [7]. In their model the motion of the cylinder is restricted to the cross-flow direction and the mass of the oscillator is quite high compared with the one in the present case (or, alternately, the surrounding fluid is much lighter). The structural frequency of the oscillator matches the natural vortex-shedding frequency at a Reynolds number of approximately 325. Computations were carried out for various Reynolds numbers in the vicinity of 325. The phenomenon of *lock-in* was observed for a range of Reynolds number. They were also able to capture the effect of *hysteresis* in their simulations and were able to explain it based on observations made by other researchers.

In this section to begin with, a summary of results is presented for the flow-induced vibrations of the cylinder when the structural frequency is equal to the natural vortex-shedding frequency (F_0) and its sub and superharmonics. Figure 3 shows the vorticity and pressure fields for the temporally periodic solution corresponding to the peak value of the lift coefficient for the oscillating cylinder. The top row shows the solution for stationary cylinder, the second row for $F_s = F_0/3$, the third one for $F_s = F_0/2$ and the fourth one for the case when the structural frequency is equal to the natural vortex-shedding frequency ($F_s = F_0$). The rest of the figure shows the solution when F_s is the second, third and fourth superharmonic of F_0. It can be noticed that the static in-line deflection of the cylinder increases as the structural frequency decreases. This is despite a significantly lower mean drag coefficient at low vibration frequencies than that at $F_s = F_0$. This behavior can be attributed to the reduction of the structural stiffness of the oscillator as the structural frequency decreases, since the mass is constant. Figure 5 shows the time histories of the drag and lift coefficients and the cylinder trajectory for various values of F_s. In the cases corresponding to $F_s = 0.07$ ($= F_0/3$) and $F_s = 0.105$ ($= F_0/2$), the cylinder vibrates mainly in the cross-flow direction. The Strouhal number corresponding to the vortex-shedding frequency and the vibration of the cylinder assumes a value that is neither equal to F_s nor F_0 but somewhere in between the two. This is also apparent from Figure 2, where one can observe that the longitudinal spacing between the vortices in the second and third rows is larger than that in the first row for stationary cylinder. Figure 6 shows the vorticity and pressure fields at five time instants during one cycle of cross-flow vibration of the cylinder for the periodic solution when $F_s = 0.21$ ($= F_0$). The time histories of the drag and lift coefficients, cylinder displacements and phase plots for this case are shown in Figure 7. This solution has been computed with mesh M2. The flow picture, corresponding to this case, in Figure 3 has been obtained with the coarser mesh of M1. On comparing the two solutions it can be observed that near-field solutions obtained from both the meshes is quite similar, while the far-wake appears to be more dissipated for the one computed on the coarse mesh (M1). Time histories of the displacements of the cylinder and the lift and drag coefficients computed with the two meshes show very close values. This is consistent with the observation that the near-field solutions are quite similar. The amplitude of cross-flow vibrations are an order of magnitude larger than those in the in-line direction. Therefore, the flow field obtained with

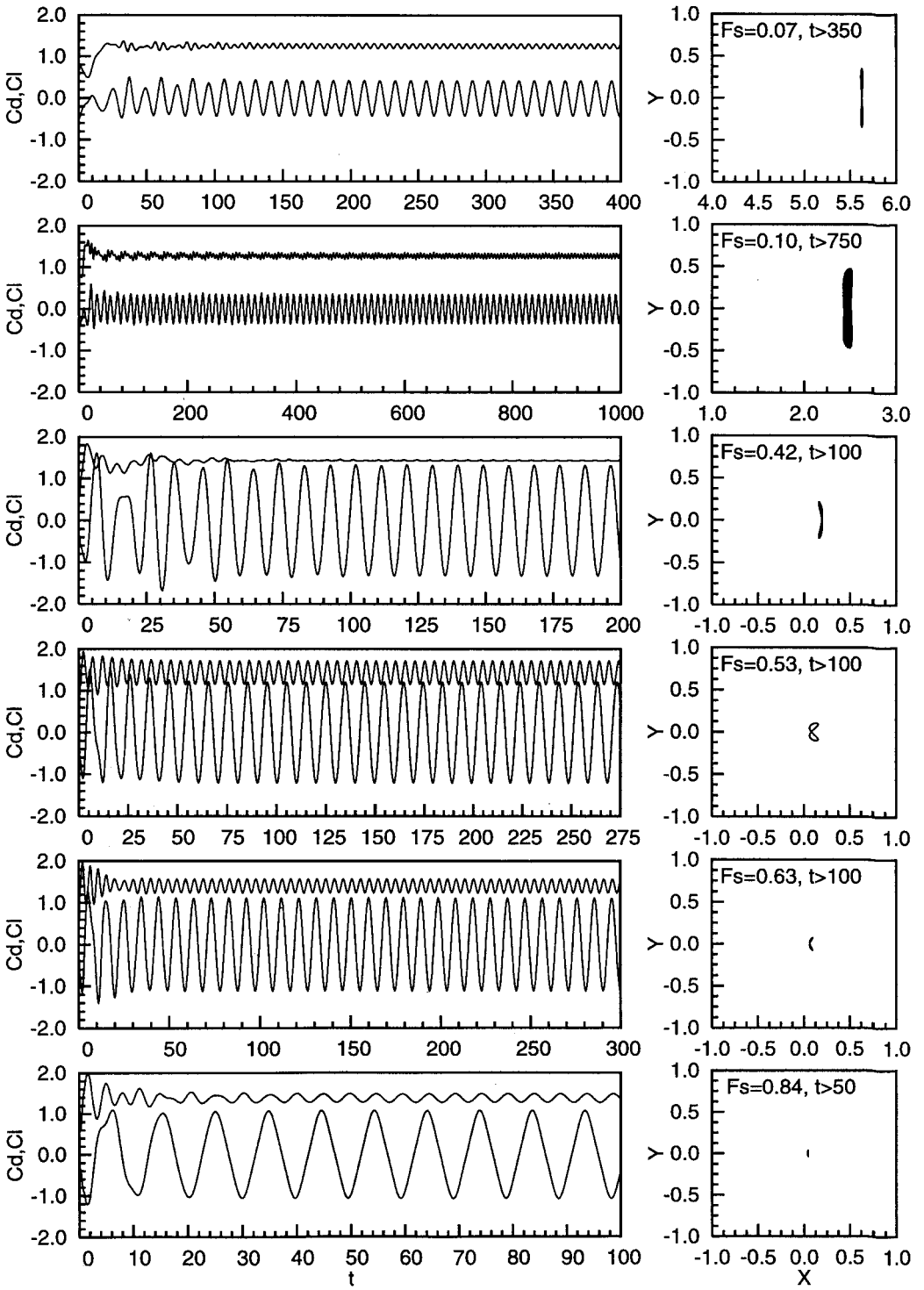

Figure 5. $Re = 325$ flow past an oscillating cylinder with $F_s = 0.07$ ($= F_0/3$), $F_s = 0.105$ ($= F_0/2$), $F_s = 0.42$ ($= 2F_0$), $F_s = 0.53$ ($= 2.5F_0$), $F_s = 0.63$ ($= 3F_0$) and $F_s = 0.84$ ($= 4F_0$): time histories of the drag and lift coefficients and cylinder displacements.

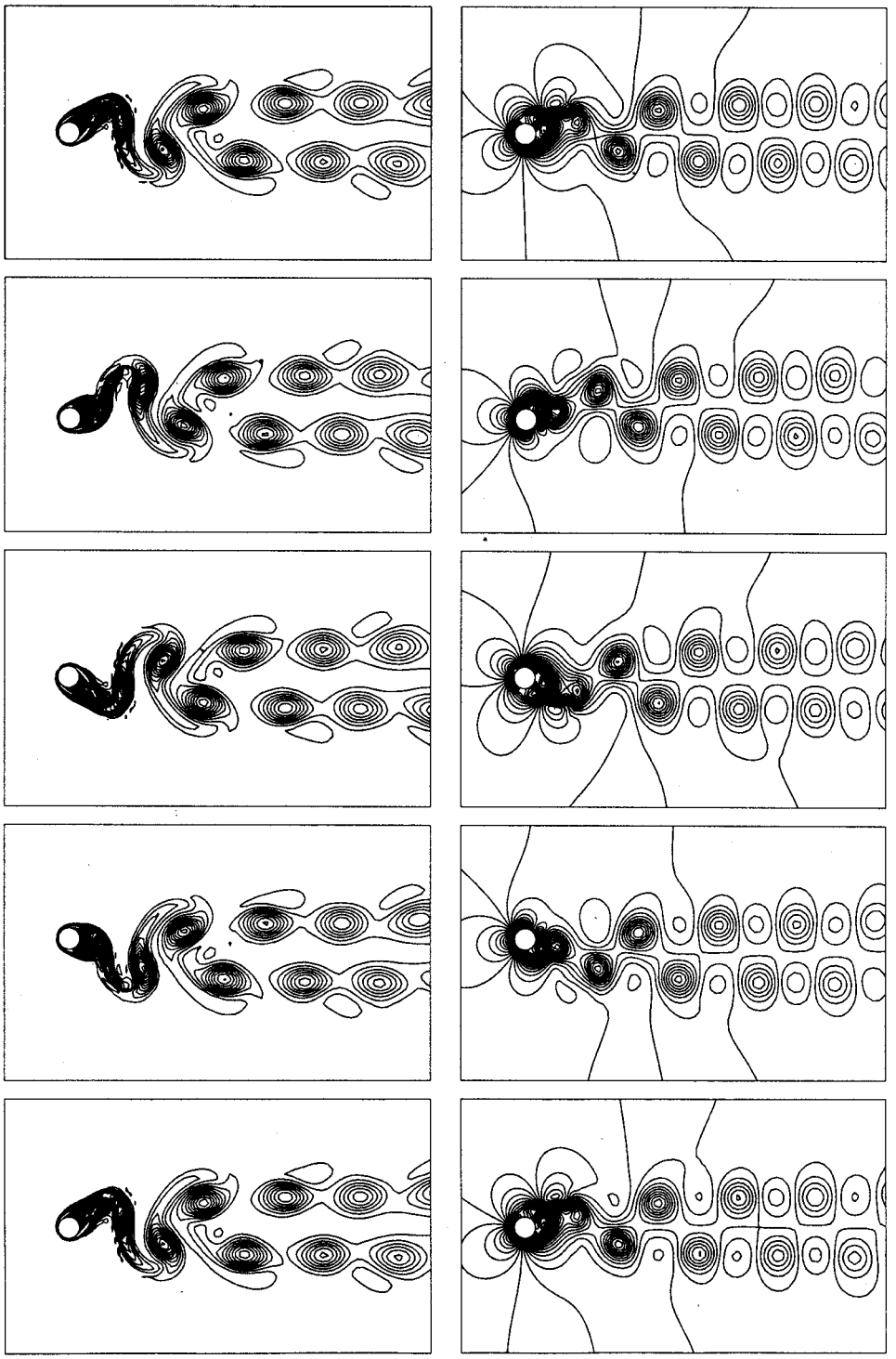

Figure 6. $Re = 325$ flow past an oscillating cylinder with $F_s = 0.21$ $(= F_0)$ computed on mesh M2: vorticity and pressure fields at five time instants during one cycle of cross-flow vibration of the cylinder for the periodic solution.

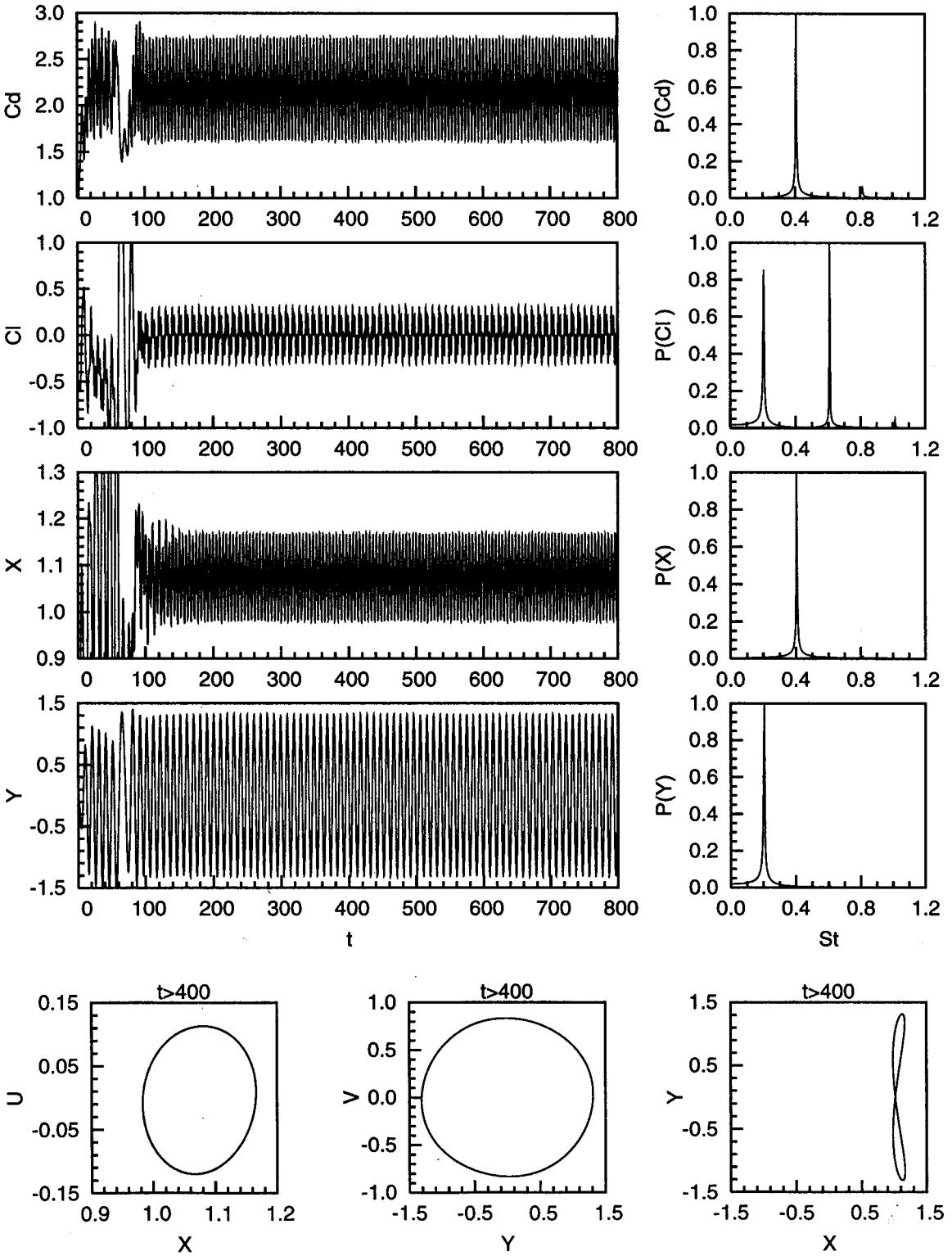

these computations is very close to the one that is seen for a cylinder whose motion is restricted to the cross-flow vibrations [7]. As a result of these vibrations the drag coefficient for the cylinder increases while the lift coefficient decreases and an additional frequency ($3F_0$) can be observed in its power spectrum. The frequency of the cross-flow oscillations is equal to the structural frequency of the oscillator. As expected, since the drag force experienced by the cylinder oscillates at twice the frequency of the lift force, the in-line vibrations are at twice the cross-flow oscillation frequency of the oscillator. The trajectory of the cylinder corresponds to a *Lissajou* figure of 8. Same observations have been made earlier by researchers during laboratory experiments [1,2]. As has been observed earlier [3,7,32], the oscillations of the cylinder are self-limiting, i.e. as the amplitude of cross-flow oscillations increases, the time-varying component of the lift coefficient reduces so that the amplitude of cross-flow vibrations do not increase beyond a certain value. An additional frequency appears in the power spectrum of the lift coefficient the effect of which is, perhaps, again to limit the cross-flow oscillations. The remaining rows in Figure 5 show the time histories of the drag and lift coefficients and the cylinder displacement for the cases with $F_s = 0.42$, 0.53, 0.63 and 0.84. The flow fields for the oscillating cylinder with F_s equal to superharmonics of F_0 are quite similar to the one observed for a stationary cylinder. Computations for $F_s = 0.53$ ($= 2.5F_0$) reveal similar behavior.

In the remaining part of this section, efforts will be concentrated on the study of the oscillator for values of F_s close to the natural vortex-shedding frequency, F_0. Figure 8 shows the vorticity and pressure fields at five time instants during one cycle of cross-flow vibration of the cylinder for the periodic solution when $F_s = 0.18$. The time histories of the drag and lift coefficients and cylinder displacements for this case are shown in the first row of Figure 9. This solution has been computed with mesh M2. The flow pictures, corresponding to the computations for the same case with the coarser mesh M1, for the peak value of the cross-flow displacement, are shown in Figure 10. *Lock-in* is observed in this case and the cylinder exhibits cross-flow vibrations with a frequency F_s and in-line oscillations with a frequency $2F_s$. The cylinder motion corresponds to a *Lissajou* figure of 8. The solutions obtained from both the meshes, M1 and M2, are quite similar except that the solution on mesh M1 appears a little dissipated as compared with the one computed on mesh M2. Compared with the solution for stationary cylinder, the longitudinal spacing between the vortices in the present case is higher. This observation is consistent with the one made by Koopmann [5] in course of his experiments with forced cross-flow vibrations of cylinders and with the computations of Mittal and Tezduyar [7]. During *lock-in*, the vortex-shedding frequency matches the cylinder oscillation frequency. It is less than F_0 in this particular case ($F_s = 0.18$). Therefore, in the present case, fewer number of vortices are shed in a given time interval compared with the fixed cylinder case (or for the oscillating cylinder when $F_s = F_0$). This causes an increase in the longitudinal spacing between the shed vortices in the wake. Similarly, for $F_s > F_0$ the longitudinal spacing between the vortices decreases if *lock-in* occurs. The time histories of the drag and lift coefficients and cylinder displacements for the computations with $F_s = 0.19$, 0.20, 0.22 and 0.23 are shown in Figure 9. *Lock-in* is observed for all the cases. However, for $F_s = 0.22$ and 0.23, the vortex-shedding frequency locks on to a value ($= 0.21$ for $F_s = 0.22$ and 0.216 for $F_s = 0.23$) that is slightly lower than F_s. We have already referred to this phenomenon as *soft-lock-in*. The cross-flow vibration frequency of the cylinder corresponds to the vortex-shedding frequency while that in the in-line direction is twice this value. The flow pictures for

Figure 7. $Re = 325$ flow past an oscillating cylinder with $F_s = 0.21$ ($= F_0$) computed on mesh M2: time histories of the drag and lift coefficients, cylinder displacements, their power spectra and phase plots.

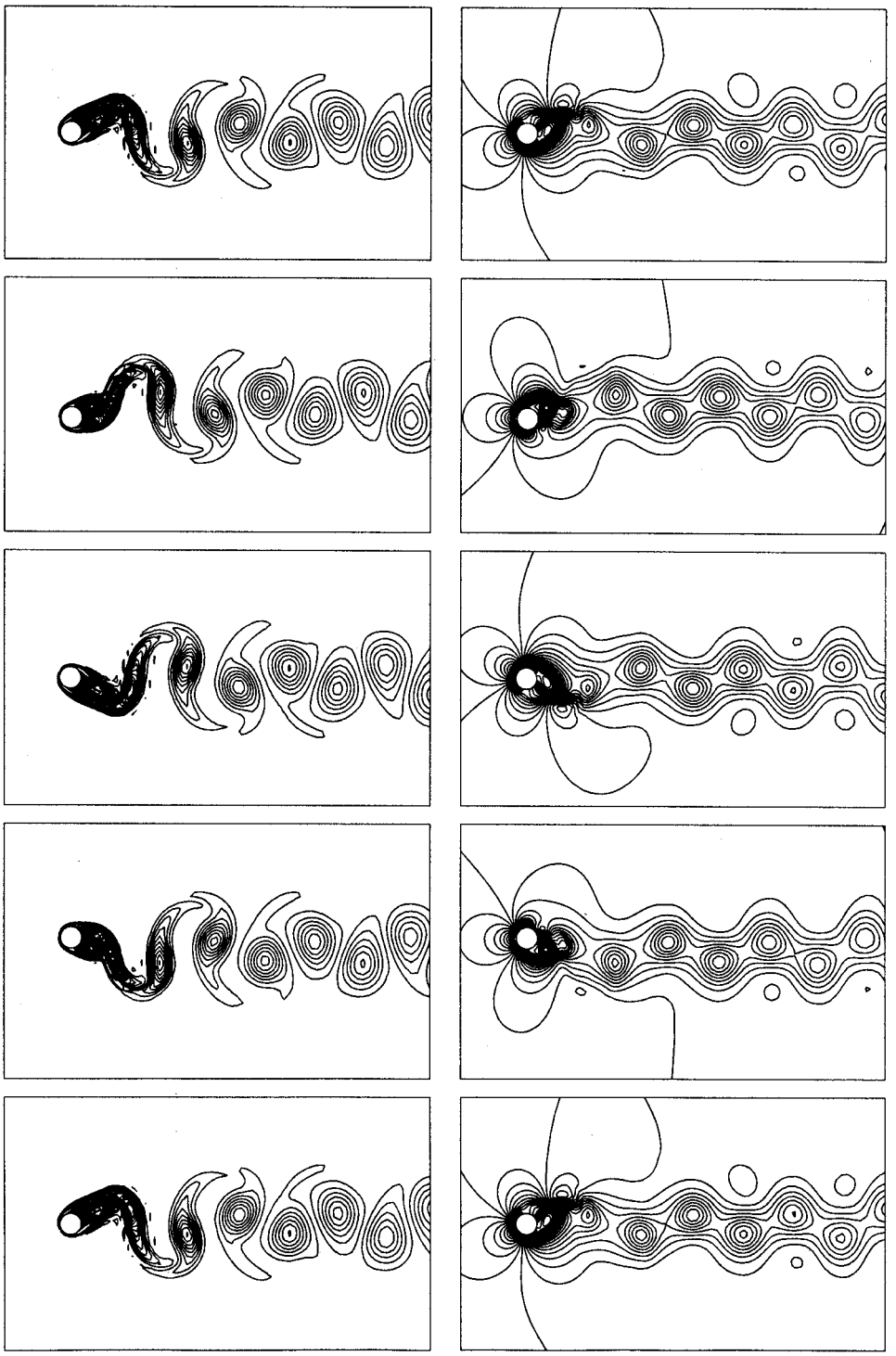

Figure 8. $Re = 325$ flow past an oscillating cylinder with $F_s = 0.18$ computed on mesh M2: vorticity and pressure fields at five time instants during one cycle of cross-flow vibration of the cylinder for the periodic solution.

$F_s = 0.23$ computed with mesh M2 are shown in Figure 11 for one cycle of the cylinder motion while that computed with mesh M1, for the peak value of the cross-flow displacement, are shown in Figure 12. As in the previous cases, the solutions computed on mesh M1 and M2 are quite similar in the near wake but different in the far wake. The solution on mesh M1 seems

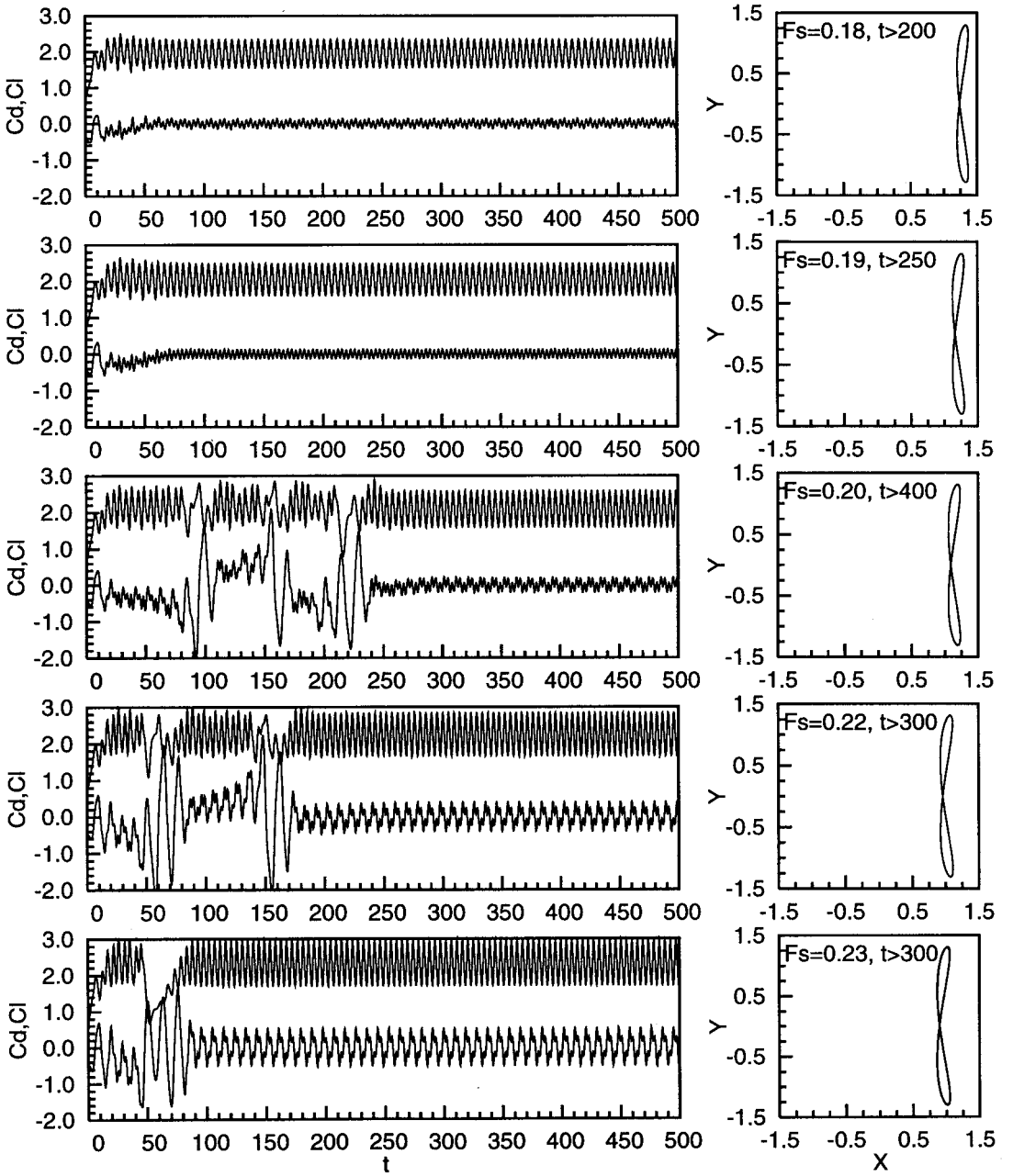

Figure 9. $Re = 325$ flow past an oscillating cylinder with $F_s = 0.18$, 0.19, 0.20, 0.22 and 0.23 computed on mesh M2: time histories of the drag and lift coefficients and cylinder displacements.

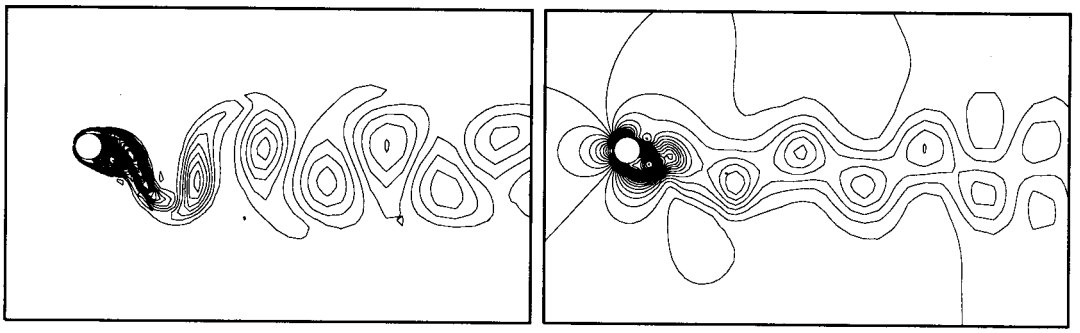

Figure 10. $Re = 325$ flow past an oscillating cylinder with $F_s = 0.18$ computed on mesh M1: vorticity and pressure fields at the peak value of the cross-flow displacement of the cylinder for the periodic solution.

to suggest that the vortices that are a few diameters downstream of the cylinder in the wake coalesce. The solution on mesh M2 clearly shows that this is not true. To ascertain that this is an artifact of spatial resolution, the solution from mesh M2 is projected on a much finer mesh M3 and computations are continued. Figure 13 shows the streamwise variation of the 'y' component of velocity at $y/D = 1.25$ for the various meshes at the peak value of the cross-flow displacement of the cylinder. Recall, that the center of the undisplaced cylinder coincides with the origin. It can be seen from the figure that the near-wake solution, from all the three meshes, is almost identical. Further downstream, in the wake region, the solution from mesh M1 appears to be quite dissipated, while those from meshes M2 and M3 are quite comparable. The time histories of the aerodynamic coefficients and the cylinder displacements obtained with all the three meshes are almost indistinguishable.

The solutions for $F_s = 0.26$ are shown in Figures 14 and 15, while those for $F_s = 0.27$ are shown in Figures 16 and 17. These cases are extremely interesting. The computations are initiated on mesh M1. After a certain time has elapsed, the solution is projected onto mesh M2 ($t = 333$ for $F_s = 0.26$ and $t = 753$ for $F_s = 0.27$) and computations are continued. For these two cases, qualitatively different solutions are observed with the two meshes. Computations on mesh M1 do not lead to *lock-in* for both the cases while the situation is quite different with mesh M2. The solution obtained with mesh M2 is projected on an even finer mesh (M3) and computations are continued. Figure 18 shows the comparison of the time histories obtained with the meshes M2 and M3. It can be observed that the solutions from the two meshes are very close, which reinforces our confidence in the solutions obtained with M2. Figure 19 shows the streamwise variation of the 'y' component of velocity at $y/D = 1.25$ for the various meshes at the peak value of the cross-flow displacement of the cylinder. Unlike the case with $F_s = 0.23$, it can be seen from the figure that the solution obtained with mesh M1 is quite different than the ones obtained with the other two more refined meshes, even in the near-wake. The solutions for meshes M2 and M3 are almost identical in the near-wake, but further downstream the solution from mesh M2 is marginally diffused compared with the one from M3. This suggests that the mesh M1, which was adequate for lower values of F_s, is insufficient to resolve the flow structures for higher values of F_s. The cause of this behavior is related to the phenomenon of *lock-in*. For larger values of F_s, when *lock-in* occurs, the longitudinal spacing between the vortices decreases and, consequently, for a fixed size of the domain more number of grid points are needed to resolve the wake adequately. *Soft-lock-in* is observed for $F_s = 0.26$ and $F_s = 0.27$, i.e. the vortex-shedding frequency is detuned from the structural frequency. It is 0.230 for $F_s = 0.26$ and 0.232 for $F_s = 0.27$. Despite the detuning, the cylinder continues to

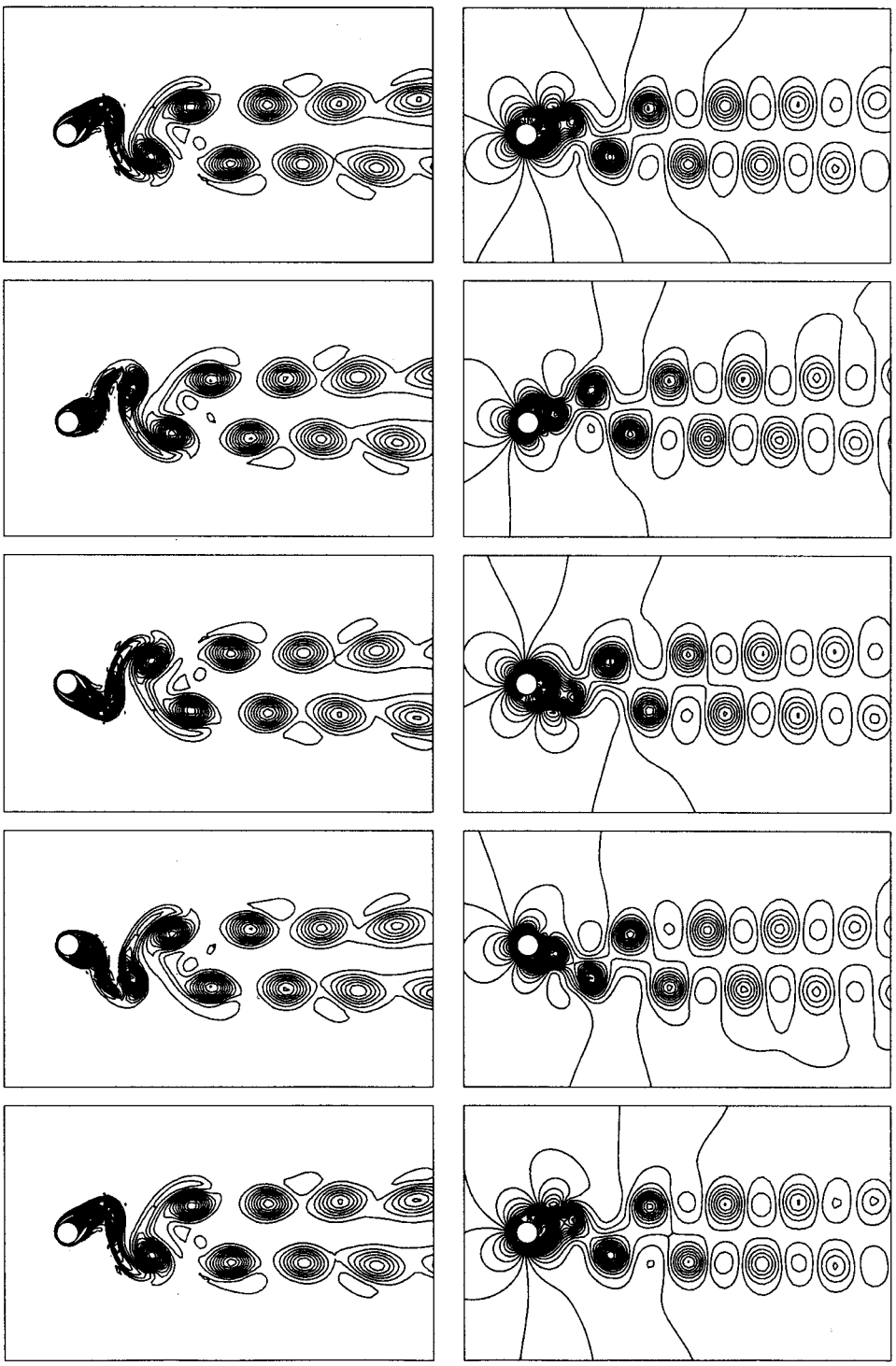

Figure 11. $Re = 325$ flow past an oscillating cylinder with $F_s = 0.23$ computed on mesh M2: vorticity and pressure fields at five time instants during one cycle of cross-flow vibration of the cylinder for the periodic solution.

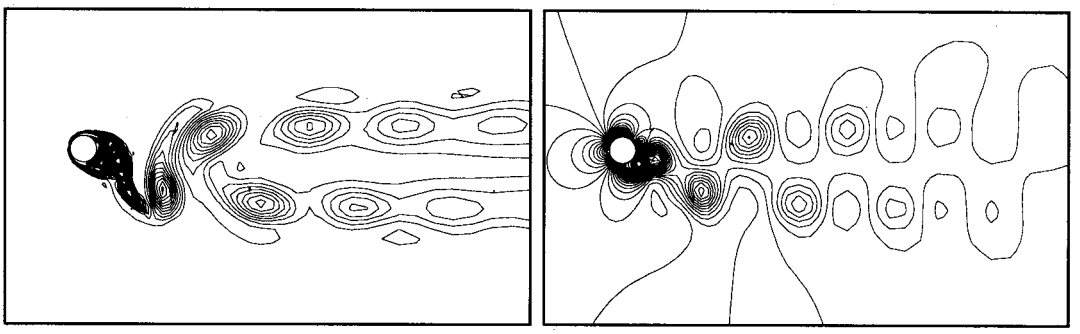

Figure 12. $Re = 325$ flow past an oscillating cylinder with $F_s = 0.23$ computed on mesh M1: vorticity and pressure fields at the peak value of the cross-flow displacement of the cylinder for the periodic solution.

exhibit large amplitude cross-flow oscillations with frequency equal to the vortex-shedding frequency.

Figure 20 shows the time histories of the drag and lift coefficients, cylinder displacements and phase plots for $F_s = 0.32$. The computations are initiated with mesh M1. At $t = 357$ the solution is projected to mesh M2 and computations are continued. It can be observed that there are both low and high frequency components in the time histories of all the quantities. The dominant frequency in the time variation of the lift force is 0.23. Unlike the previous cases, lock-in is not observed and the trajectory of the cylinder motion does not follow a figure of 8. The dominant frequency in the time variation of both the in-line and cross-flow vibrations is 0.46. Figures 21 and 22 show the flow fields during one cycle of the cylinder motion in the cross-flow direction for small and large amplitude cycles respectively. The two sets of flow pictures are quite different and represent two modes of vortex-shedding. The figures showing the time histories also suggest a competition between the two modes. It should also be mentioned that the solution remains virtually the same when it is projected from the mesh M2 to mesh M3 and the computations are continued. The qualitative nature of the solutions obtained from all the three meshes is very similar. Computations for $F_s = 0.35$ also exhibit mode competition. The solution computed on mesh M1 is shown in Figure 23. The amplitude of cross-flow vibrations is much lower than in the other cases. The presence of two

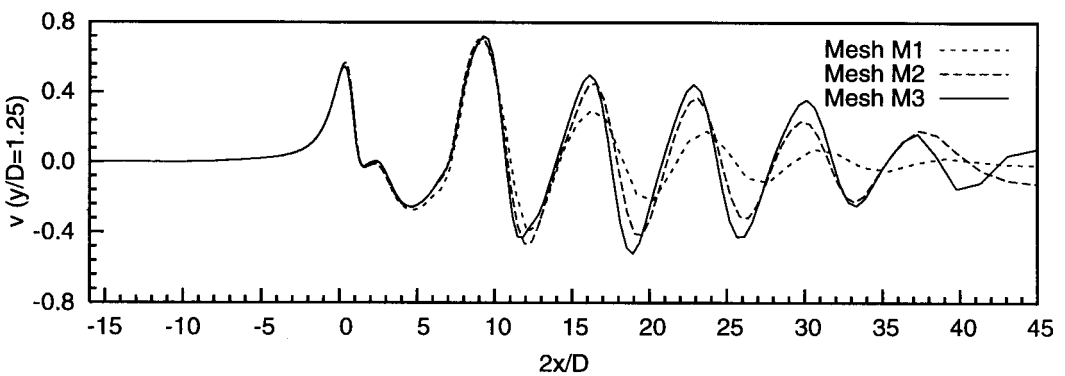

Figure 13. $Re = 325$ flow past an oscillating cylinder with $F_s = 0.23$: variation of the y component of velocity at $y/D = 1.25$ corresponding to the peak value of the cross-flow displacement of the cylinder for various meshes. The center of the undisplaced cylinder lies at the origin.

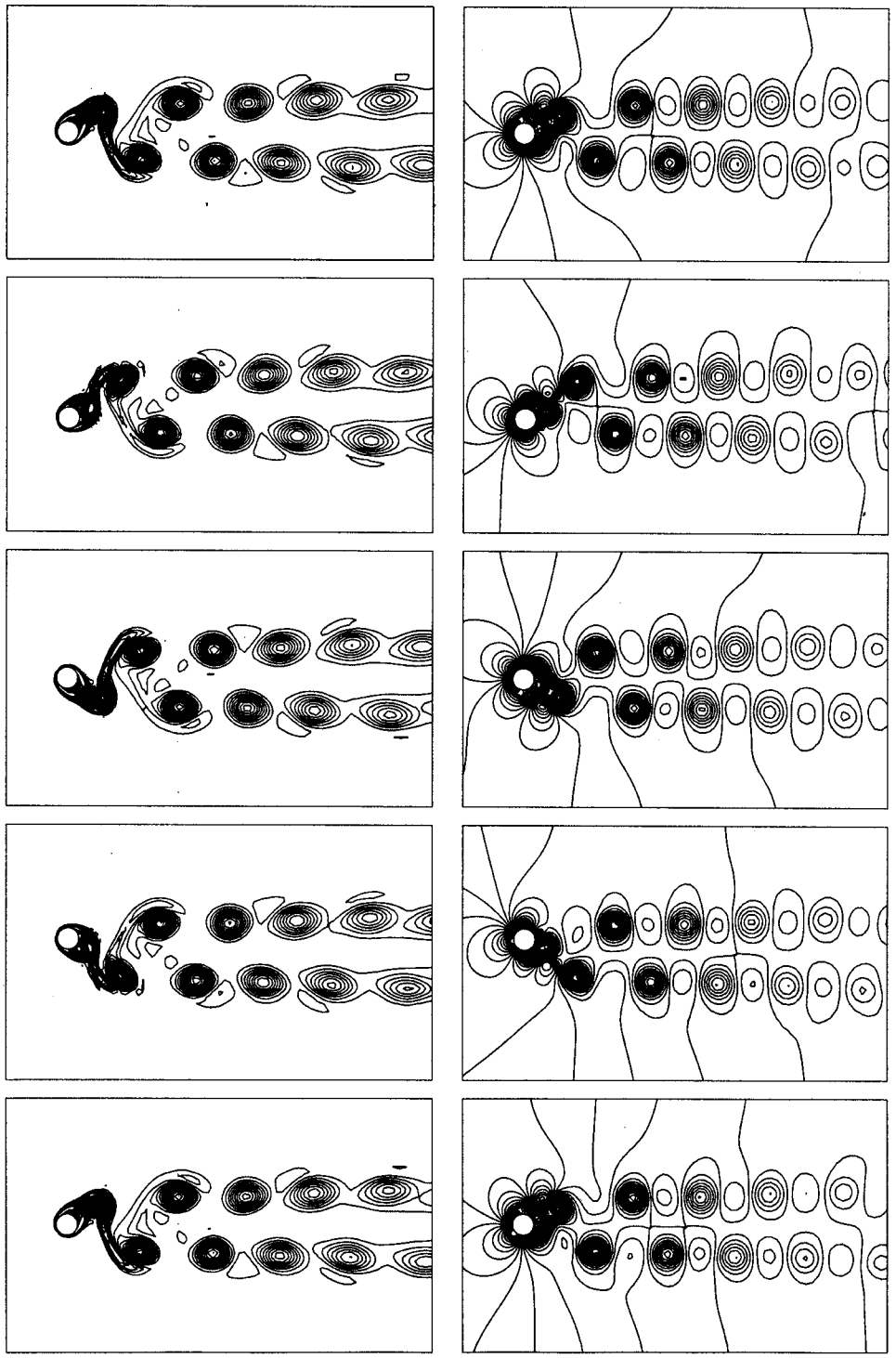

Figure 14. $Re = 325$ flow past an oscillating cylinder with $F_s = 0.26$ computed on mesh M2: vorticity and pressure fields at five time instants during one cycle of cross-flow vibration of the cylinder for the periodic solution.

distinct peaks in the power spectrum of the time history of the lift coefficient is an additional evidence for the presence of two modes of vortex-shedding, one at a low frequency (close to that for a stationary cylinder) and the other at a higher frequency (approximately 0.23), which is the maximum that has been observed for the oscillating cylinder, for the present computations. It is an interesting observation that any significant effect of the mesh on the unsteady solution is noticed only in a small window of values of F_s close to 0.27. This observation supports the reason for mesh dependence of the solution that was suggested earlier in this section.

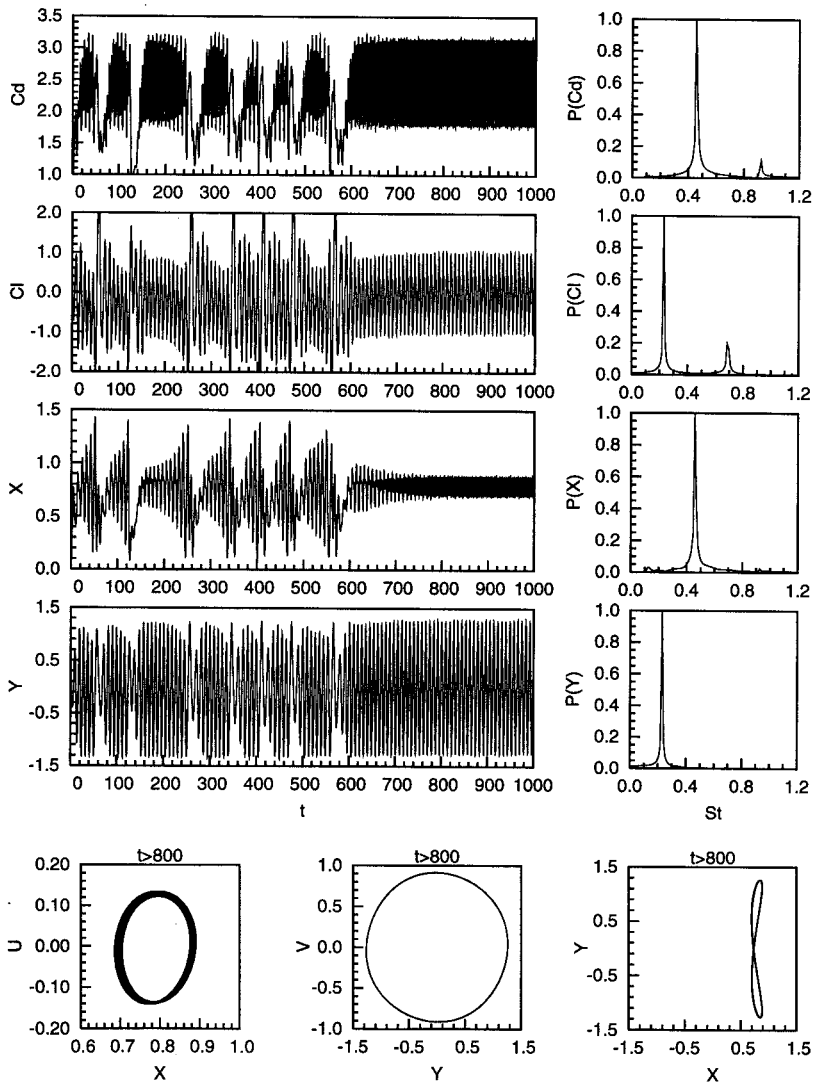

Figure 15. $Re = 325$ flow past an oscillating cylinder with $F_s = 0.26$ computed on mesh M1 for $t < 333$ and on mesh M2 for $t > 333$: time histories of the drag and lift coefficients, cylinder displacements, their power spectra and phase plots.

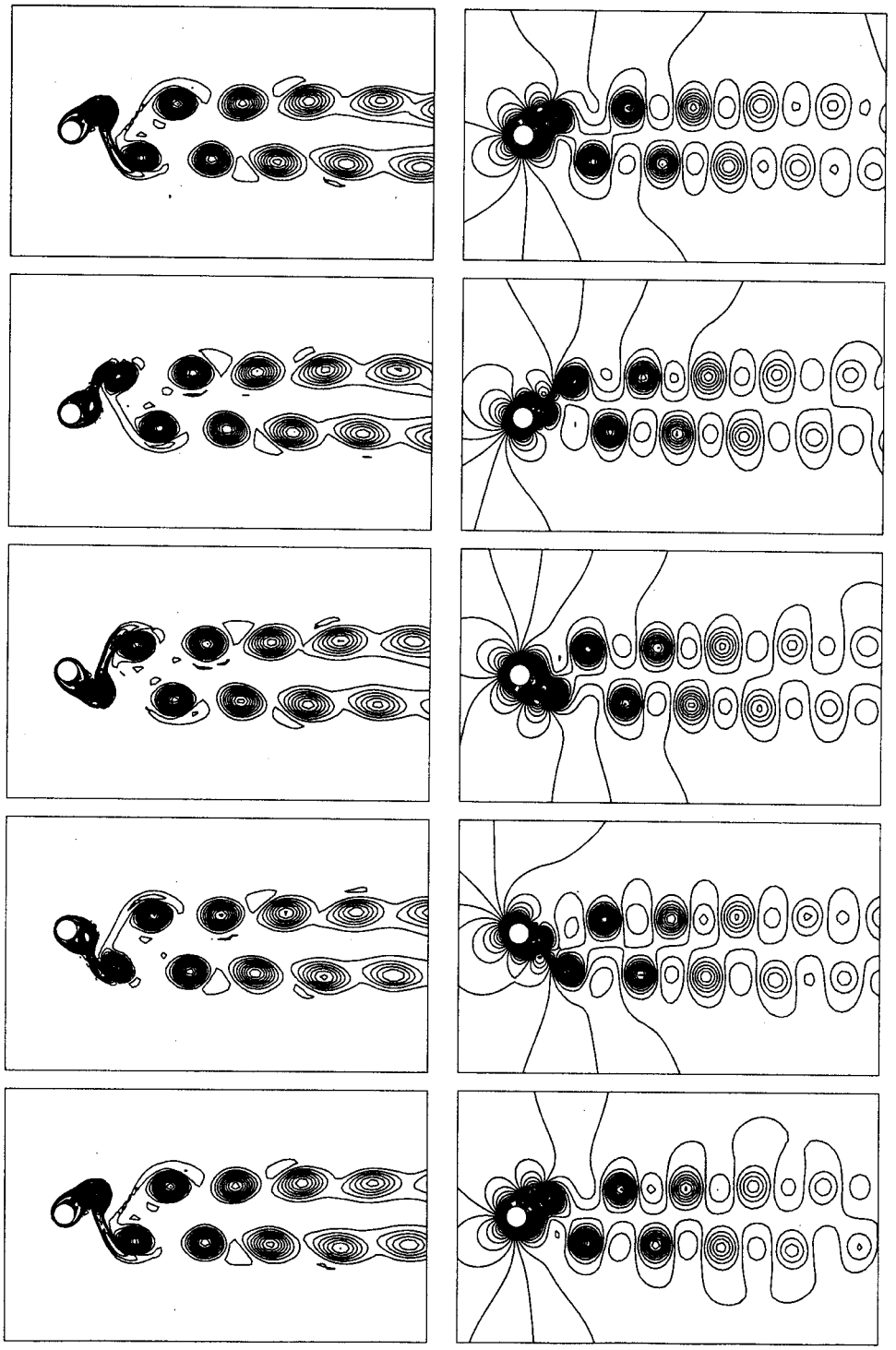

Figure 16. $Re = 325$ flow past an oscillating cylinder with $F_s = 0.27$ computed on mesh M2: vorticity and pressure fields at five time instants during one cycle of cross-flow vibration of the cylinder for the periodic solution.

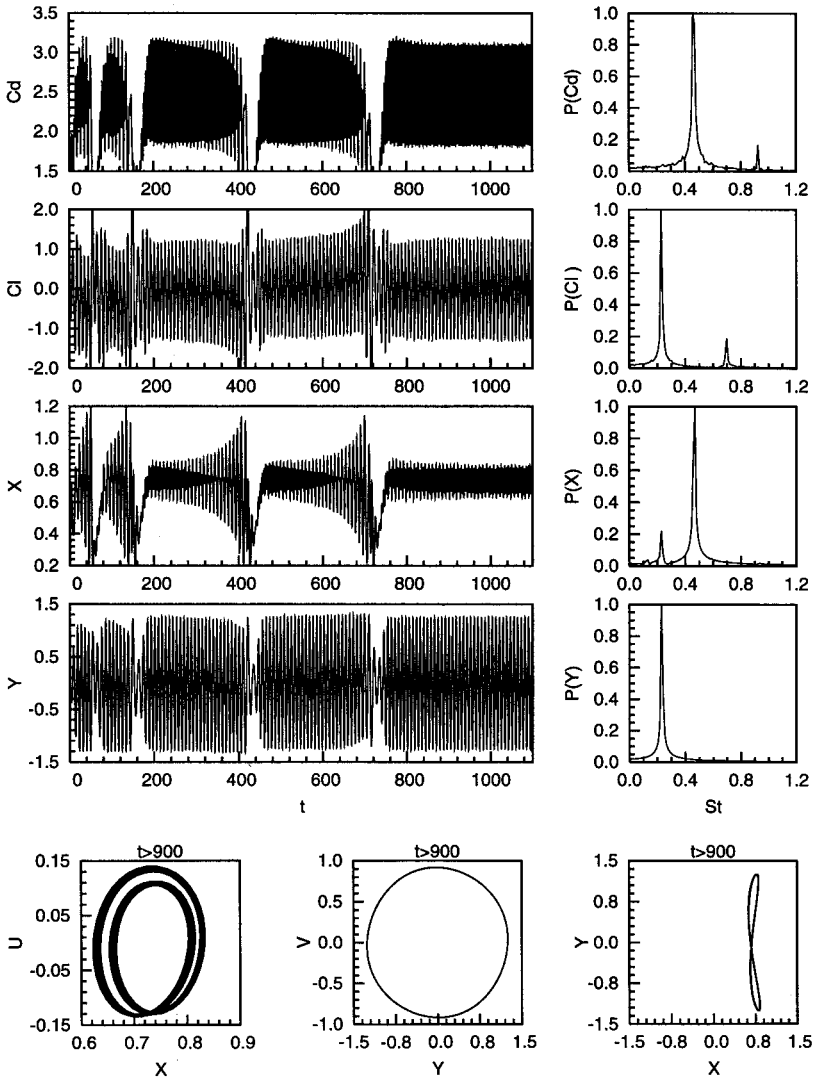

Figure 17. $Re = 325$ flow past an oscillating cylinder with $F_s = 0.27$ computed on mesh M1 for $t < 753$ and on mesh M2 for $t > 753$: time histories of the drag and lift coefficients, cylinder displacements, their power spectra and phase plots.

4.3. $F_s = 0.25$, $Re = 325$ flow past an oscillating cylinder: effect of oscillator mass

It was observed in the previous section that for certain values of F_s, the vortex-shedding frequency for an oscillating cylinder assumes a value that is somewhere in between the natural vortex-shedding frequency for stationary cylinder and the structural frequency. We have referred to this phenomenon as *soft-lock-in*. The cylinder, as expected, oscillates with the vortex-shedding frequency. To investigate the cause of this behavior, the effects of oscillator mass and the restriction of its motion to cross-flow vibrations is studied. It is seen from our computations (the results are not presented here) that the restriction of the motion of the cylinder to the cross-flow vibrations does not affect the results. *Soft-lock-in* is still observed.

The next parameter to be studied is the mass of the oscillator. The top row of Figure 24 shows the time histories of the drag and lift coefficients and the cylinder displacements for $F_s = 0.25$ and for the mass of the oscillator as in the previous section ($M = 4.73$) computed with mesh M2. The solution looks quite similar to the one obtained in the previous section for $F_s = 0.26$. The frequency of vortex-shedding and the cross-flow vibrations of the cylinder is 0.227. The solutions obtained for an increased mass of the oscillator ($M = 25.0$) are shown in the second row of Figure 24. It is observed that the increase in mass leads to a reduced amplitude of in-line oscillations. However, there is no change in the amplitude of cross-flow vibrations. It should be noticed that the amplitude of vibrations observed by Mittal and Tezduyar [7] for an oscillator that is a hundred times heavier than the present one is comparable with that in the current case. This is a very interesting behavior and reflects the self-limiting nature of the flow-induced vibrations. The vortex-shedding frequency of the oscillator with the increased mass is 0.245. We observe that, as the mass of the oscillator increases, the vortex-shedding frequency approaches the structural frequency. This suggests that it is the mass of the cylinder that is responsible for the phenomenon of *soft-lock-in*. Of course, if the mass of the oscillator

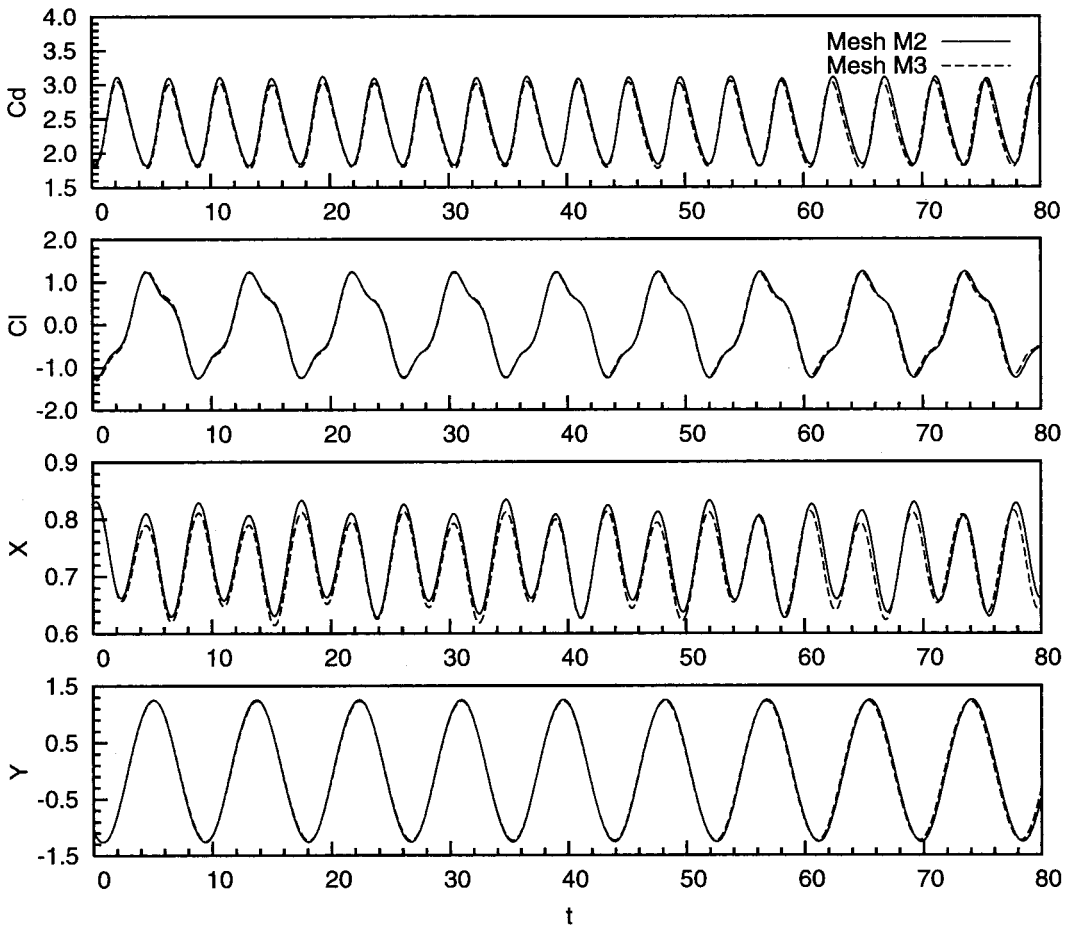

Figure 18. $Re = 325$ flow past an oscillating cylinder with $F_s = 0.26$: comparison of the time histories of the drag and lift coefficients and cylinder displacements computed on the meshes M2 and M3.

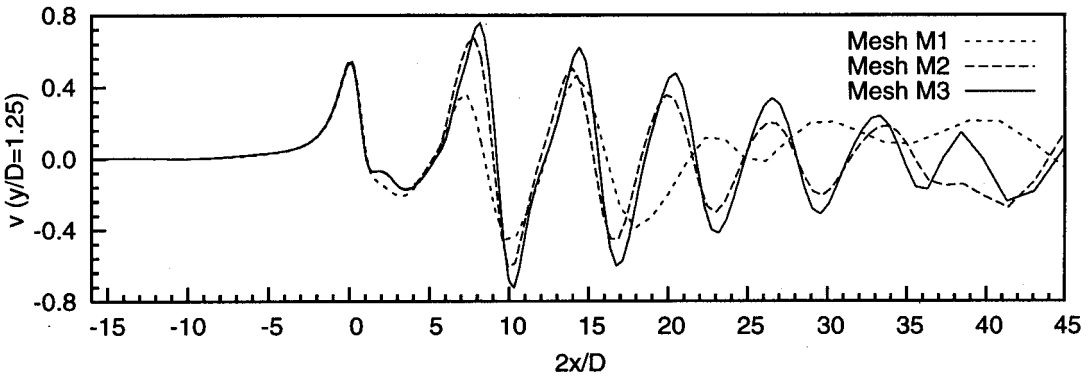

Figure 19. $Re = 325$ flow past an oscillating cylinder with $F_s = 0.26$: variation of the y component of velocity at $y/D = 1.25$ corresponding to the peak value of the cross-flow displacement of the cylinder for various meshes. The center of the undisplaced cylinder lies at the origin.

is increased beyond a certain value, the oscillator would cease to lock-in and the range of values of the structural frequency for which lock-in occurs would be reduced to a narrower band. The results presented by Cetiner and Unal [33] suggest a similar trend. It is our belief, based on several observations made by us and other researchers in the past, that the various mechanisms by which the oscillator is able to self-limit its cross-flow vibrations are by a reduction in the lift force amplitude, appearance of additional frequency components in the time histories of the lift force and detuning of the vortex-shedding frequency from the structural frequency. The first two mechanisms are quite well known. However, to the best of our knowledge, the last mechanism has not been reported before.

5. CONCLUSIONS

Vortex-induced vibrations of a circular cylinder placed in a uniform flow at a Reynolds number of 325 have been studied using a stabilized space–time finite element formulation. The cylinder is allowed to vibrate, both in the in-line and cross-flow directions. The behavior of the oscillator for various values of the structural frequency (F_s) including those that are sub and superharmonics of the natural vortex-shedding have been presented. In most of the cases, the trajectory of the cylinder corresponds to a *Lissajou* figure of 8. The frequency of the in-line oscillations is twice of that in the cross-flow direction. Unlike some of the previous studies that reported subharmonic resonance for forced oscillations of a cylinder, our results do not reveal such behavior. The behavior of the vortex-shedding frequency of the oscillating cylinder is a little different than what is conventionally observed. It has been observed by various researchers in the past that for a certain range of the structural frequency (F_s), the vortex-shedding frequency of an oscillating cylinder locks on to F_s. This phenomenon is referred to as *lock-in*. Most of these observations have been made for cylinders whose effective material density is much larger than that of the surrounding fluid. In the present study it has been observed that over a certain range of F_s, the vortex-shedding frequency of the oscillating

Figure 20. $Re = 325$ flow past an oscillating cylinder with $F_s = 0.32$ computed on mesh M1 for $t < 357$ and on mesh M2 for $t > 357$: time histories of the drag and lift coefficients, cylinder displacements, their power spectra and phase plots.

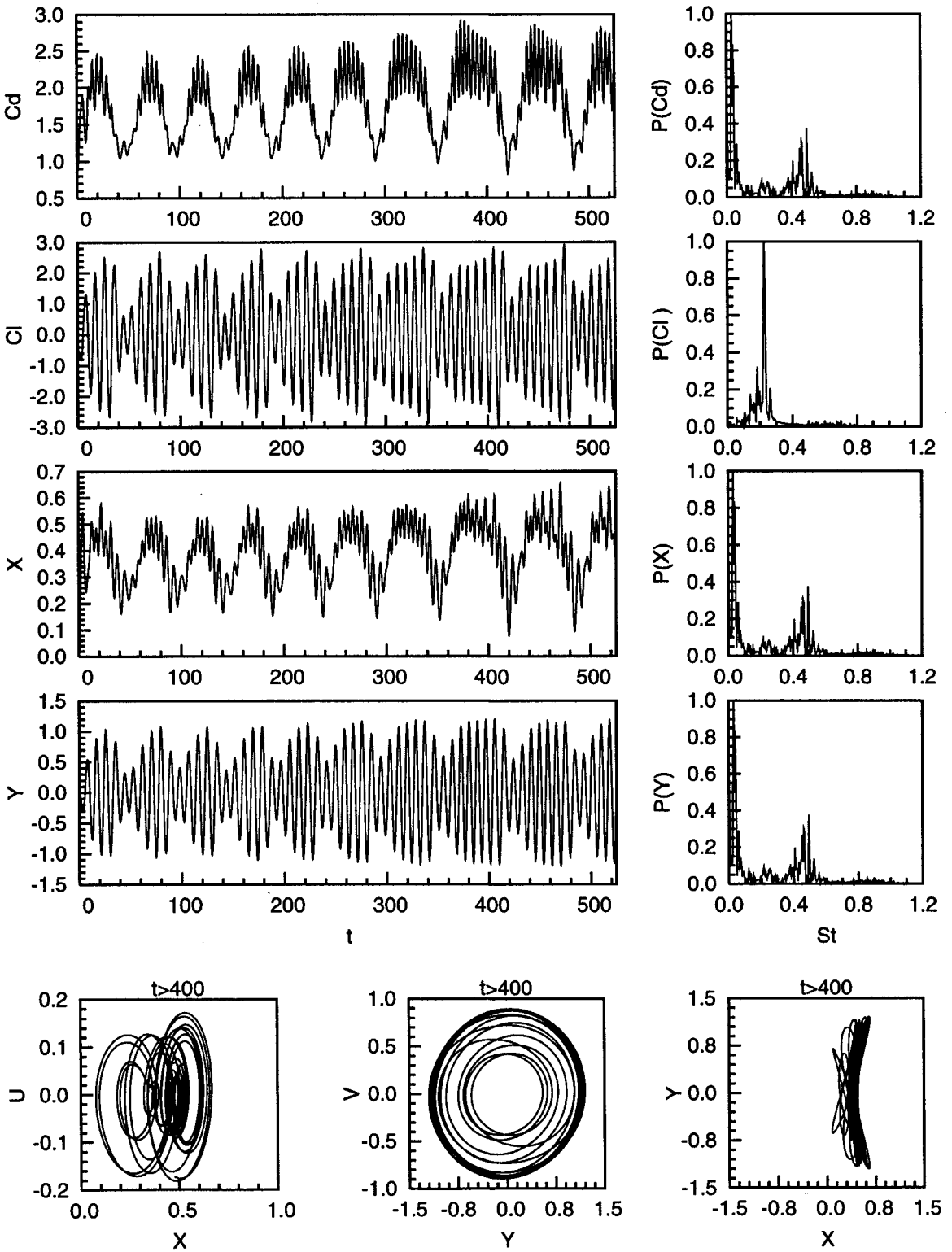

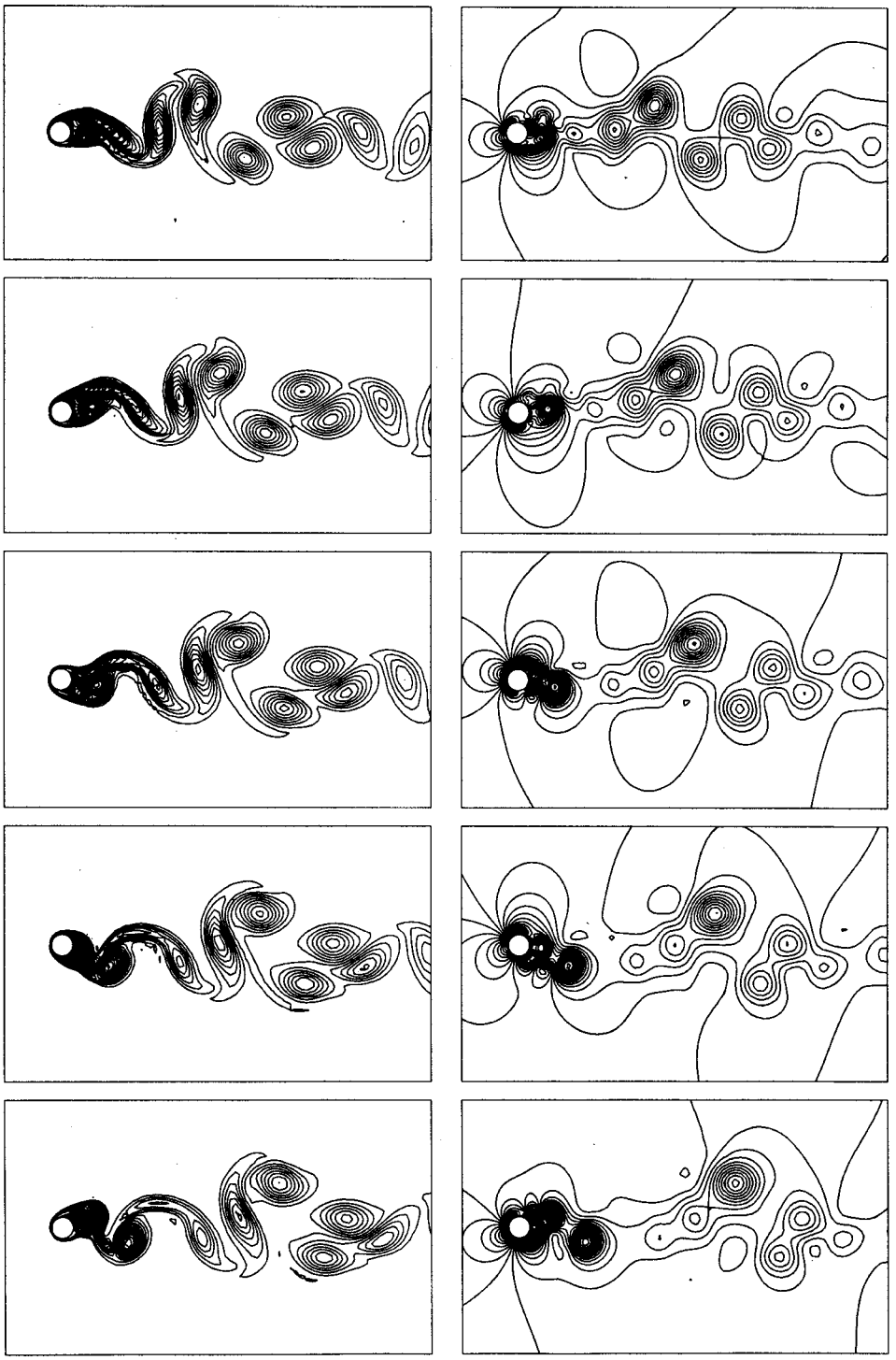

Figure 21. $Re = 325$ flow past an oscillating cylinder with $F_s = 0.32$ computed on mesh M2: vorticity and pressure fields at five time instants during one cycle of small amplitude cross-flow vibration of the cylinder.

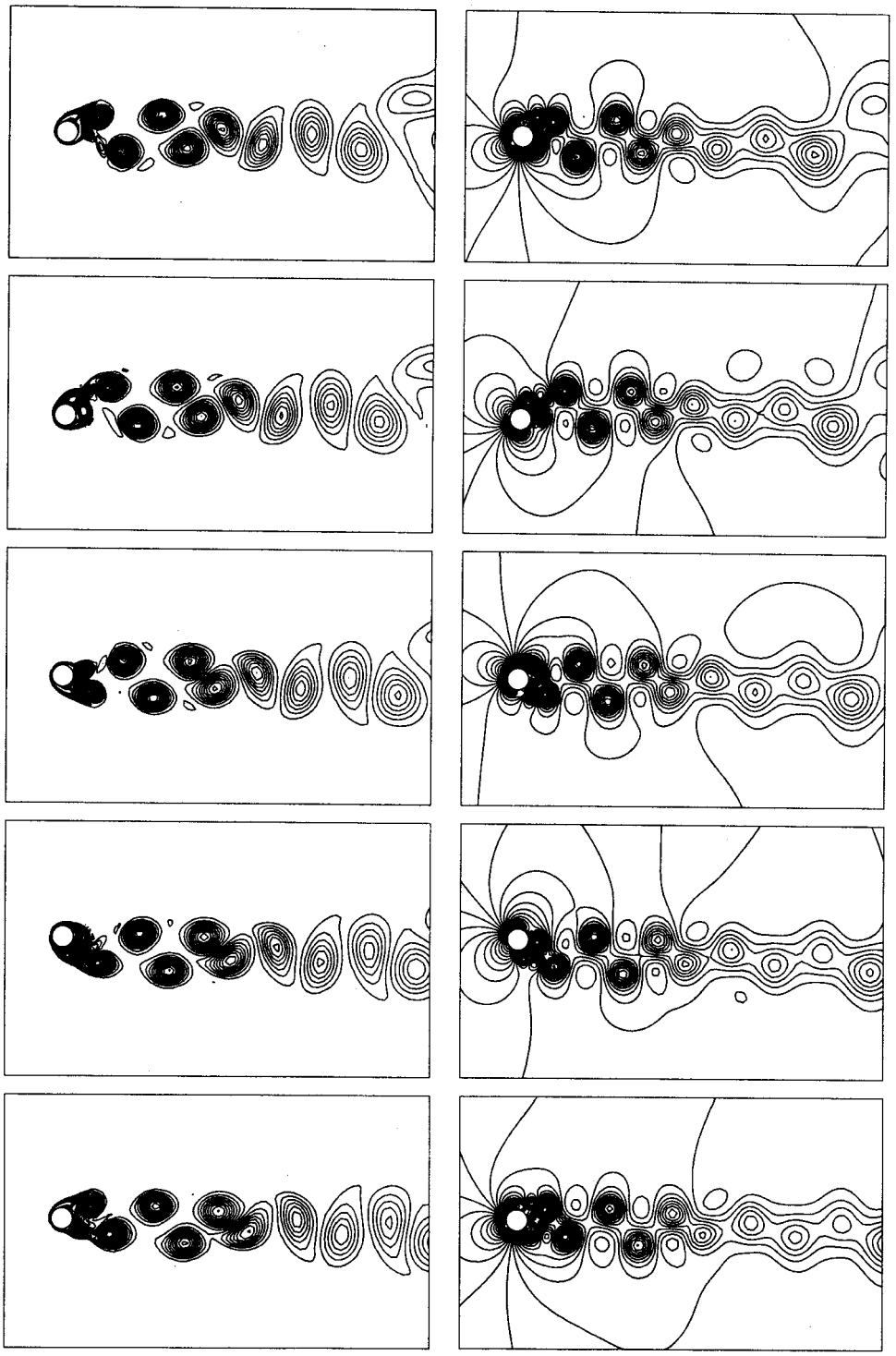

Figure 22. $Re = 325$ flow past an oscillating cylinder with $F_s = 0.32$ computed on mesh M2: vorticity and pressure fields at five time instants during one cycle of large amplitude cross-flow vibration of the cylinder.

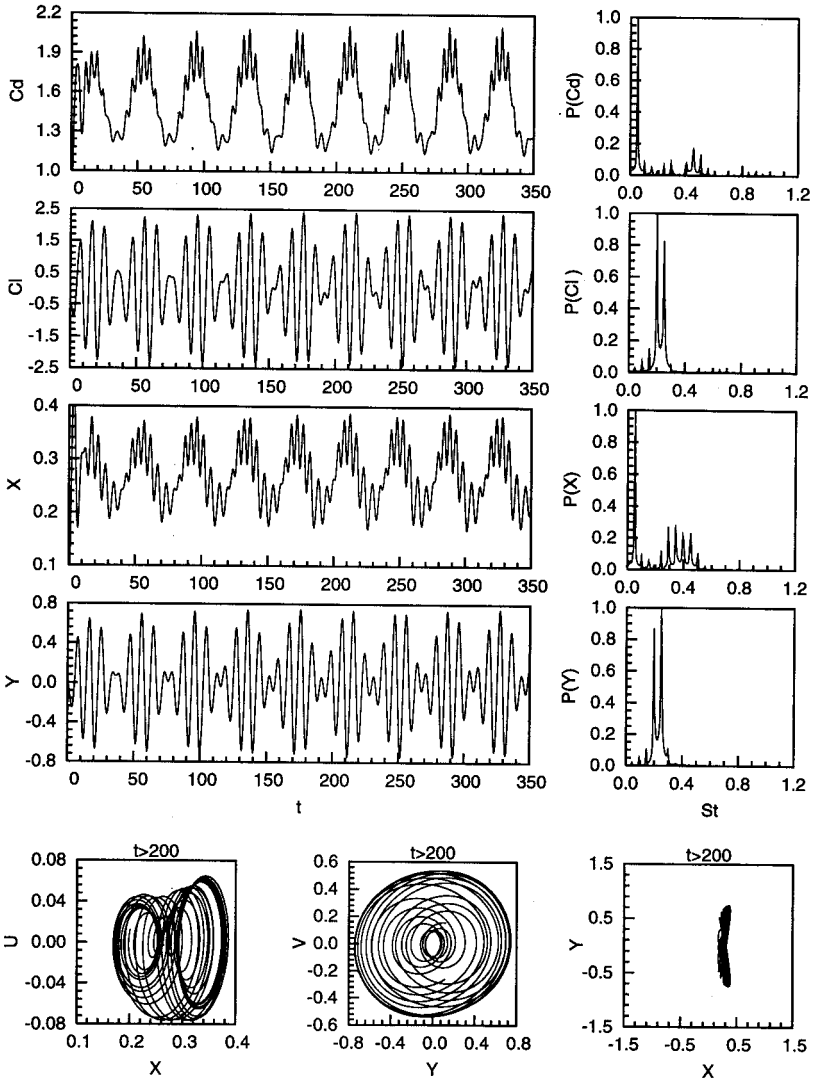

Figure 23. $Re = 325$ flow past an oscillating cylinder with $F_s = 0.35$ computed on mesh M1: time histories of the drag and lift coefficients, cylinder displacements, their power spectra and phase plots.

cylinder does not exactly match the structural frequency; there is a slight *detuning*. This phenomenon is referred to as *soft-lock-in*. Our computations show that this detuning disappears if the mass of the cylinder is much larger than the mass of the surrounding fluid it displaces. A self-limiting nature of the oscillator with respect to cross-flow vibration amplitude is observed. As the vibration amplitude increases, the flow changes and so do the aerodynamic forces acting on the cylinder to limit the amplitude of oscillation. In certain cases, even when the mass of the oscillator is reduced by two orders of magnitude, there is no appreciable change in the vibration amplitude. The detuning of the vortex-shedding frequency from the structural frequency is a mechanism of the oscillator to self-limit its vibration amplitude and, to the best of the knowledge of the authors, has not been reported before. The dependence of

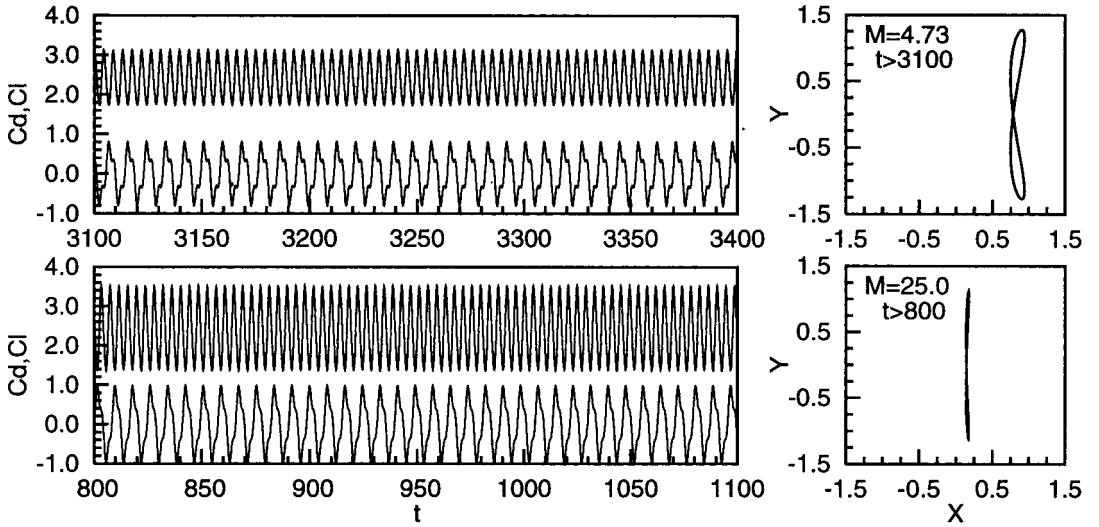

Figure 24. $Re = 325$ flow past an oscillating cylinder with $F_s = 0.25$ computed on mesh M2: time histories of the drag and lift coefficients and cylinder displacements for $M = 4.73$ and 25.0.

the unsteady solution on the spatial resolution of the finite element mesh has been investigated. Our calculations demonstrate that even though a mesh may be good enough to resolve all the flow structures at a certain Reynolds number, the same mesh in certain cases may not provide enough resolution for computing flows involving moving boundaries and interfaces.

ACKNOWLEDGMENTS

Partial support for this work has come from the Department of Science and Technology, India under the project number DST-AE-95279 with Department of Aerospace Engineering, IIT Kanpur.

REFERENCES

1. R.D. Blevins, *Flow-Induced Vibration*, Van Nostrand Reinhold, New York, 1990.
2. S.S. Chen, *Flow-Induced Vibrations of Circular Cylindrical Structures*, Hemisphere, New York, 1987.
3. T. Sarpkaya, 'Vortex-induced oscillations: a selective review', *J. Appl. Mech.*, **46**, 241–258 (1979).
4. R. King, 'A review of vortex-shedding research and its application', *Ocean Eng.*, **4**, 141–171 (1977).
5. G.H. Koopmann, 'The vortex wakes of vibrating cylinders at low Reynolds numbers', *J. Fluid Mech.*, **28**, 501–512 (1967).
6. O.M. Griffin, R.A. Skop and G.H. Koopmann, 'The vortex-excited resonant vibrations of circular cylinders', *J. Fluid Mech.*, **54**, 235–249 (1973).
7. S. Mittal and T.E. Tezduyar, 'A finite element study of incompressible flows past oscillating cylinders and airfoils', *Int. J. Numer. Methods Fluids*, **15**, 1073–1118 (1992).
8. O.M. Griffin and S.E. Ramberg, 'Vortex shedding from a cylinder vibrating in line with an incident uniform flow', *J. Fluid Mech.*, **75**, 257–271 (1975).
9. K.S. Chang and J.Y. Sa, 'Patterns of vortex shedding from an oscillating circular cylinder', *AIAA J.*, **30**, 1331–1336 (1992).
10. Y. Tanida, A. Okajima and Y. Watanabe, 'Stability of a circular cylinder in uniform flow or in a wake', *J. Fluid Mech.*, **61**, 769–784 (1973).
11. D.J. Olinger and K.R. Sreenivasan, 'Non-linear dynamics of the wake of an oscillating cylinder', *Phys. Rev. Lett.*, **60**, 797–800 (1988).
12. O.M. Griffin, 'The unsteady wake of an oscillating cylinder at low Reynolds number', *J. Appl. Mech.*, **38**, 729–738 (1971).

13. G.H. Toebes, 'The unsteady flow and wake near an oscillating cylinder', *J. Basic Eng.*, **91**, 493–505 (1969).
14. Y. Lecointe, J. Piquet and J. Plantec, 'Flow structure in the wake of an oscillating cylinder', in K.N. Ghia (ed.), *Forum on Unsteady Flow Separation*, FED-52, ASME, New York, 1987, pp. 147–157.
15. W.W. Durgin, P.A. March and P.J. Lefebvre, 'Lower mode response of circular cylinders in cross-flow', *J. Fluids Eng. Trans. ASME*, **102**, 183–190 (1980).
16. C.H.K. Williamson and A. Roshko, 'Vortex formation in the wake of an oscillating cylinder', *J. Fluids Struct.*, **2**, 355–381 (1988).
17. H. Blackburn and R. Henderson, 'Wake dynamics in flow past and oscillating cylinder', in C. Taylor and P. Durbetaki (eds.), *Numerical Methods in Laminar and Turbulent Flow*, vol. 9, Pineridge Press, Swansea, 1995, pp. 1479–1490.
18. A. Ongoren and D. Rockwell, 'Flow structure from an oscillating cylinder. Part 1. Mechanisms of phase shift and recovery in the near wake', *J. Fluid Mech.*, **191**, 197–223 (1988).
19. A. Ongoren and D. Rockwell, 'Flow structure from an oscillating cylinder. Part 2. Mode competition in the near wake', *J. Fluid Mech.*, **191**, 225–245 (1988).
20. T.E. Tezduyar, M. Behr and J. Liou, 'A new strategy for finite element computations involving moving boundaries and interfaces—the deforming spatial domain/space–time procedure: I. The concept and the preliminary tests', *Comput. Methods Appl. Mech. Eng.*, **94**, 339–351 (1992).
21. T.E. Tezduyar, M. Behr, S. Mittal and J. Liou, 'A new strategy for finite element computations involving moving boundaries and interfaces—the deforming spatial domain/space–time procedure: II. Computation of free-surface flows, two-liquid flows, and flows with drifting cylinders', *Comput. Methods Appl. Mech. Eng.*, **94**, 353–371 (1992).
22. Y. Saad and M. Schultz, 'GMRES: a generalized minimal residual algorithm for solving nonsymmetric linear systems', *SIAM J. Sci. Statist. Comput.*, **7**, 856–869 (1986).
23. T.E. Tezduyar, S. Mittal, S.E. Ray and R. Shih, 'Incompressible flow computations with stabilized bilinear and linear equal-order-interpolation velocity–pressure elements', *Comput. Methods Appl. Mech. Eng.*, **95**, 221–242 (1992).
24. S. Mittal, 'Stabilized space–time finite element formulations for unsteady incompressible flows involving fluid–body interactions', *PhD Thesis*, University of Minnesota, 1992.
25. M. Behr, J. Liou, R. Shih and T.E. Tezduyar, 'Vorticity–streamfunction formulation of unsteady incompressible flow past a cylinder: sensitivity of the computed flow field to the location of the outflow boundary', *Int. J. Numer. Methods Fluids*, **12**, 323–342 (1991).
26. M. Behr, D. Hastreiter, S. Mittal and T.E. Tezduyar, 'Incompressible flow past a circular cylinder: dependence of the computed flow field on the location of the lateral boundaries', *Comput. Methods Appl. Mech. Eng.*, **123**, 309–316 (1995).
27. H. Schlichting, *Boundary-Layer Theory*, 7th edn., McGraw-Hill, New York, 1979.
28. S. Balachandar and R. Mittal, 'Role of three-dimensionality in the near wake of two-dimensional cylinders', in T.S. Mruthyunjaya (ed.), *Mechanics and Thermal Sciences*, *Advances in Mechanical Engineering*, vol. II, Narosa Publishing House, Indian Institute of Science Bangalore, India, 1996, pp. 1385–1395.
29. V. Kalro and T. Tezduyar, 'Parallel finite element computation of 3D incompressible flows on mpps', in W.G. Habashi (ed.), *Solution Techniques For Large-Scale CFD Problems*, Computational Methods in Applied Sciences, Wiley, New York, 1994; also in *Proceedings of the International Workshop on Solution Techniques for Large-Scale CFD Problems*, Montreal, Quebec, Canada.
30. C.H.K. Williamson, 'Oblique and parallel modes of vortex shedding in the wake of a circular cylinder at low Reynolds numbers', *J. Fluid Mech.*, **206**, 579–627 (1989).
31. C.H.K. Williamson, 'Vortex dynamics in the cylinder wake', *Annu. Rev. Fluid Mech.*, **28**, 477–539 (1996).
32. O.M. Griffin and G.H. Koopmann, 'The vortex-excited lift and reaction forces on resonantly vibrating cylinders', *J. Sound Vibrat.*, **54**, 435–448 (1977).
33. N.L.O. Cetiner and M.F. Unal, 'A discrete vortex study of vortex-induced oscillations of a circular cylinder', in C. Taylor and P. Durbetaki (eds.), *Numerical Methods in Laminar and Turbulent Flow*, vol. 9, Pineridge Press, Swansea, 1995, pp. 1467–1478.

